

COUPLING AND STATE TRANSFER IN
JOSEPHSON QUBIT SYSTEMS

Inauguraldissertation

ZUR

ERLANGUNG DER WÜRDE EINES DOKTORS DER PHILOSOPHIE

VORGELEGT DER

PHILOSOPHISCH-NATURWISSENSCHAFTLICHEN FAKULTÄT

DER UNIVERSITÄT BASEL

VON

ANDRIY LYAKHOV

AUS DER UKRAINE

BASEL, 2008

GENEHMIGT VON DER PHILOSOPHISCH-NATURWISSENSCHAFTLICHEN FAKULTÄT
AUF ANTRAG VON PROF. DR. CHRISTOPH BRUDER UND PROF. DR. ROSARIO
FAZIO

BASEL, DEN 16.10.2007

PROF. DR. HANS-PETER HAURI

DEKANIN/DEKAN

Declaration

I, Andriy Lyakhov, confirm that the work presented in this thesis is my own. Where information has been derived from other sources, I confirm that this has been indicated in the thesis.

© Copyright by Andriy Lyakhov, 2008.

All Rights Reserved

Abstract

The quantum information science (QIS) is relatively young, but quite broad and emerging field of modern physics. This is an interdisciplinary field where quantum mechanics, computer science, mathematics and computing technologies meet together. Using the laws of quantum mechanics to deal with information opens many new opportunities. However, these opportunities can only be used if one can construct a quantum logic device to implement QIS methods. In the last decade many researchers proposed the variety of physical systems, that can be used as building blocks of the so called quantum computer. But the question of building an effective connection between different blocks remains open. Recently, the idea to build a 'quantum wire' using chains of permanently coupled spins was studied by a number of authors. The purpose of this thesis is to investigate and develop advanced schemes for using quantum chains as wires. The first part of the thesis shortly describes the concepts of quantum computing and quantum state transfer. We then briefly introduce different schemes to couple two superconducting qubits and analyze more closely one of them. Then we analyze the process of the state transfer for the chain of flux qubits. Next, we propose a new method of improved quantum state transfer which was created as a part of this thesis. Finally, we study the effects and the role of interference in quantum state transfer via spin chains.

Acknowledgements

First of all, I would like to gratefully acknowledge my supervisor Christoph Bruder whose kind support and guidance made my thesis work possible. Together with D. Braun, F. Paauw and D. Burgarth I had numerous fruitful discussions, more or less related to this thesis. Furthermore I would like to thank my teachers who motivated me to study physics. Big thanks to members of Condensed Matter Group in Basel University for making my staying in Basel so enjoyable. And last but not least, I would like to thank my parents and girlfriend for their loving support.

Contents

Declaration	iii
Abstract	iv
Acknowledgements	v
1 Introduction	1
1.1 Quantum computing	1
1.2 Quantum spin chains as transmission lines	6
1.3 Heisenberg Hamiltonian	11
1.4 Improved quantum state transfer in spin chains	12
1.5 Outline	17
2 Coupling of two superconducting qubits	18
2.1 Introduction	18
2.2 Static coupling between qubits	19
2.2.1 Techniques to realize two qubit gates with static coupling between qubits	23
2.3 Parametric coupling for superconducting qubits	26
2.4 Dynamical coupling between qubits using additional circuits	27
2.4.1 Circuits to couple charge qubits	27
2.4.2 Circuits to couple flux qubits	31
2.5 Conclusion	33
3 Variable coupling scheme for superconducting charge qubits	34
3.1 Introduction	34
3.2 Born-Oppenheimer-like approximation	34
3.3 Numerical results	37

3.4	Conclusion	45
4	Quantum state transfer in arrays of flux qubits	47
4.1	Introduction	47
4.2	Persistent-current qubit arrays	47
4.3	Fidelity of the state transfer	55
5	Use of dynamical coupling for improved quantum state transfer	63
5.1	Introduction	63
5.2	Time-dependent coupling constants	64
5.3	Conclusion	73
6	Quantum interference in the state transfer via spin chains	74
6.1	Introduction	74
6.2	Quantum interference	75
6.3	Role of quantum interference in the state transfer	76
6.3.1	Interference and reduced interference	76
6.3.2	Reduced interference for excitation-conserving spin chains	77
6.3.3	Chains that conserve the number of excitations	80
6.3.4	Chains that do not conserve the number of excitations	83
6.3.5	Interference in the unitary propagation of the entire chain	85
6.4	Conclusion	89
7	Conclusion and outlook	91

1 Introduction

1.1 Quantum computing

In this section we will shortly describe the concepts of quantum computing and quantum state transfer. A classical computer has a memory made up of bits, where each bit holds either one or zero. A quantum computer maintains a sequence of qubits. A qubit (quantum bit) is a two-level quantum system. Therefore it can exist not only in the state corresponding to the logical state 0 or 1 as in a classical bit, but also in states corresponding to any superposition of these classical states

$$A_0|0\rangle + A_1|1\rangle, \tag{1}$$

allowing infinite number of states.

This unique property of quantum bit gives quantum computers the potential to be incredibly powerful computational devices. However, we can not say that quantum tools will speed up different information processing tasks by a uniform amount. Some tasks are not sped up at all by using quantum tools [1], some are sped up moderately (Grover algorithm for locating an entry in database) and some are sped up exponentially (Shor's algorithm for factoring an integer number for which only exponential classical algorithms are known at this time).

To measure the effectiveness of a machine doing some specific task, the so called time complexity measure is used. The time complexity of a problem is a number of steps that it takes to solve an instance of the problem on a machine as a function of the size of the input (usually measured in bits), using the most efficient algorithm. Big O notation is generally used (sometimes described as the "order" of the calculation, as in "on the order of"). If a problem has time complexity $O(n^2)$ (an instance that is n bits long that can be solved in n^2 steps) on one typical computer, then it will also have complexity $O(n^2)$ on other computers, so this notation allows us to

generalize away from the details of a particular computer. For example painting a fence has linear time complexity ($O(n)$) because it takes double time to paint double area. However, searching a number in a yellow page book has only logarithmic time complexity ($O(\log n)$) because double sized book only has to be opened one time more (e.g. exactly in the middle - then the problem size is reduced by half). There is a whole branch of the theory of computation in computer science, *computational complexity theory*, that describes the scalability of algorithms, and the inherent difficulty in providing scalable algorithms for specific computational problems.

In the terms of computational complexity theory, using the quantum computer for searching the entry in the database speeds up the task from $O(n)$ to $O(n^{1/2})$ compared to classical computer. Factorizing the integer speeds up from exponential time complexity $O(\exp((\log n)^{2/3}n^{1/3}))$ for the fastest known classical algorithm to $O((\log n)^3)$. This turns out to be one of the practically important tasks, since the hardness of this problem is the heart of several widely used cryptographic systems. For example a fast integer factorization algorithm would mean that the RSA public-key algorithm, used in the web-security and in most electronic commerce protocols, is insecure.

Using the laws of quantum mechanics, instead of classical physics, we do not only speed up tasks that are solvable on classical computers. Naturally, there are tasks that are not doable in the classical world at all. For example quantum cryptography uses quantum mechanics to guarantee absolute secure communication, that is impossible to implement using any classical algorithm. There are also tasks that naturally suits quantum computers. For example, Richard Feynman asserted that a quantum computer could function as a kind of simulator for quantum physics. Although a classical computer can theoretically do the same, it is very inefficient, so that a classical computer is effectively incapable of performing many tasks that a quantum computer could perform easily. For example a system of only thirty qubits that exists in the

Hilbert space of dimension $\sim 10^9$ in simulation would require a classical computer to work with extremely large matrices (to perform calculations on each individual state, which is also represented as a matrix), meaning it would take an exponentially longer time than even a simple quantum computer.

A quantum computer is a device that performs unitary operations with quantum registers (sequences of n qubits that is the quantum mechanical analogue of a classical processor register). The contents of the qubit registers can be thought of as an n -dimensional complex vector. An algorithm for a quantum computer must initialize this vector in some specified form (dependent on the design of the quantum computer). In each step of the algorithm, that vector is modified by multiplying it by the unitary matrix. The matrix is determined by the physics of the device. The unitary character of the matrix ensures the matrix is invertible (so each step is reversible). Upon termination of the algorithm, the n -dimensional complex vector stored in the register must be somehow read off from the qubit register by a quantum measurement.

We have to mention, that physical qubits can be (and quite often are) represented by the physical system with more than 2 possible states. However it is usually assumed, that probability of the system to ever go in any state save the first two can be neglected. If this probability is sufficiently small, quantum error correction can "repair" the qubit. In this thesis we will consider physical qubits as quantum two-level systems.

There are a number of quantum computing candidates:

- Superconductor-based quantum computers (including SQUID-based quantum computers)
- Trapped ion quantum computer
- "Nuclear magnetic resonance on molecules in solution"-based quantum computers

- "Quantum dot on surface"-based quantum computers
- "Cavity quantum electrodynamics" (CQED)-based quantum computers
- Solid state NMR Kane quantum computers
- Optic-based quantum computers

Different proposals have different strong and weak sides and at the moment we can not claim any of them to be the best one. And probably there will be more proposals in the nearest future, that will allow us to perform quantum computing tasks. To guide the search for a feasible quantum computing architecture the set of five general criteria was developed. These five criteria, called DiVincenzo criteria [2], say that for a system to be a candidate for an implementation of quantum computation, it should

1. Be a scalable physical system with well-defined qubits.
2. Be initializable to a simple fiducial state such as $|000\dots\rangle$.
3. Have long relevant decoherence times, much longer than the gate operation time.
4. Have a universal set of quantum gates.
5. Permit high quantum efficiency, qubit-specific measurements.

These criteria are sufficient for quantum computation *per se*. But to build good and scalable quantum computer we would also like to be able to communicate between different parts of it. Also, ability to perform quantum communication (transmit qubits from place to place) is an essential part of many tasks in quantum information processing. For example, algorithms for secret key distribution, secret sharing, multi-party function evaluation as in appointment scheduling, etc. Therefore two additional criteria are often considered as necessary to build a quantum computer [2]:

6. The ability to interconvert stationary and flying qubits.
7. The ability to faithfully transmit flying qubits between specified locations.

We will now briefly discuss the five main DiVincenzo criteria. The first one describes two basic properties of the system, that are required for efficient implementation of quantum computation. Qubits are necessary to store the quantum information that would be manipulated during the computation. Well defined qubit means that its physical parameters (such as Hamiltonian, presence of and coupling to other states of the qubit, etc) are accurately known. Scalability is important if we want to build an universal quantum computer. Non scalable proposals could allow us to solve some specific problem, but you can not solve other problems and, thus, quantum computer will not be universal. For example, Shor's algorithm, mentioned above, was realized using nuclear magnetic resonance (NMR) on ensembles of molecules in liquids [3]. The number 15 was factored into 3 and 5. However, the NMR-based quantum computing proposal is not scalable and therefore you cannot factorize numbers higher than 15 using that particular type of molecules or execute any quantum algorithm that requires more than 4 qubits.

The second criterion simply means that we should be able to initialize our qubit register to some known value before the start of computation.

The third criterion means that during the computation time no quantum information should be lost and our quantum computing should not be reduced to classical one. The decoherence time characterizes the dynamics of qubit in contact with its environment and describes the time-scale for the emergence of classical behavior.

The fourth criterion basically determines if the system is a quantum computer, i.e. a device that can perform arbitrary unitary operations with the qubits. Fortunately, any such operation can be expressed in terms of sequences of one- and two-qubit interactions [4] and the two-body interactions can be just one type [5]. It means that we can achieve universal quantum computation using small amount of gates: a few

single-qubit gates and one two-qubit gate. There are also proposals where quantum information tasks are performed without using any gates, for example, measurement based quantum computing using cluster states [6, 7]. But all other criteria must still be satisfied for those proposals as well.

The fifth criterion implies that we can read out the result of a computation, as this implies the ability to measure specific qubits.

The last two criteria use the term "flying qubit", i.e. the qubit that can be transmitted from one position in space to another. It can be a moving physical qubit (for example photon or electron) or a logical qubit that is transmitted through the array of physical qubits with fixed positions. The purpose of this research is to study the transfer of quantum information through chains of permanently coupled flux Josephson qubits, to improve existing ideas for the transfer of quantum information by using time dependent end gates and to investigate the role of coherence and interference in high-quality state transfer.

1.2 Quantum spin chains as transmission lines

Recently, the idea to use quantum spin chains for short-distance quantum communication was put forward by Bose [8]. He showed that an array of spins (or spin-like two level systems) with isotropic Heisenberg interaction is suitable for quantum state transfer. The advantage of spin chains as transmission lines is the fact, that they do not need to have controllable couplings between the qubits or complicated gating schemes to achieve high transfer fidelity. For simplicity we will assume the case of linear chains with sender having access to the first and receiver having access to the last spin in the chain. In general one can consider graphs of qubits with sender and receiver having access the subgraphs of this graph in the same way like we do with the linear chain. We will also consider mostly chains where Hamiltonians conserve the number on excitations. Since we start with at most one excitation in the chain

this will reduce significantly the dimensionality of the Hilbert space of a quantum chain that we are interested in (from 2^N to $N + 1$). This allows us to derive some analytical results in studying chain dynamics and makes numerical calculations for longer chains much easier.

In the following we use the terms spin and qubit as equivalent. State $|1\rangle$ in qubit language (which we will also call “excitation”) corresponds to spin-up in spin language, and state $|0\rangle$ corresponds to spin-down.

The basic communication protocol, proposed in [8], can be described in several simple steps:

1. The chain is initialized in its ground state

$$|\psi_0\rangle = |0\dots 0\rangle \quad (2)$$

where all the spins are in their ground states. This is an important step since any excitation left in the chain will interfere with the state to be transmitted and will decrease the quality of the chain transfer drastically. How this initialization can be achieved in particular systems will be discussed later.

2. At time $t = 0$, the sender initializes the first spin of the chain in some unknown state

$$|\psi_{in}\rangle = \cos\frac{\theta}{2}|0\rangle + e^{i\phi}\sin\frac{\theta}{2}|1\rangle \quad (3)$$

We are talking about unknown state, because if the state to be transferred is known it can be simply reproduced by the receiver.

3. After a certain time t_1 receiver measures (or picks up in any way) the state

$$|\psi_{out}\rangle = Tr_{1,\dots,N-1}e^{-iHt_1}|\phi_{in}\rangle \quad (4)$$

at his end of the chain. The fidelity of quantum communication averaged over

all pure input states on the Bloch sphere, the quantity that we derive later in this chapter, is taken as a measure of the transmission quality.

Bose showed that for short chains (number of spins $\simeq 100$) the average fidelity is quite high, greater than $2/3$, which is the highest fidelity of transmission through a classical channel [9]. In a homogeneous chain, i.e. if all coupling constants are the same, the information about the input state is dispersed between the spins at all times $t > 0$. Therefore the fidelity is always less than 1 (maximal possible value that imply an ideal state transfer) for chains with more than two spins.

Fidelity of the state transfer

Following [8] we will now derive the explicit form of the fidelity. Using the basic communication protocol we assume that the sender initializes the first spin of the chain in some unknown state (3). We perform our calculations in the basis $|k\rangle = |00\dots 010\dots 0\rangle$ for which the spin in the k -th qubit is in the state $|1\rangle$ and all the others are in the state $|0\rangle$. For the chains with Hamiltonians that conserve the number of excitations the evolution of the chain is

$$|\psi(t)\rangle = \cos \frac{\theta}{2} |\psi_0\rangle + e^{i\phi} \sin \frac{\theta}{2} \sum_{j=1}^N \langle j | e^{-iHt} | 1 \rangle | j \rangle . \quad (5)$$

Now following step 3 described above we will trace out all the spins except the last one from $|\psi(t)\rangle$ to receive the state (possibly mixed) of the receiver spin.

$$\rho_{out} = p(t) |\psi_{out}\rangle \langle \psi_{out}| + (1 - p(t)) |0\rangle \langle 0| \quad (6)$$

where

$$|\psi_{out}\rangle = \frac{1}{\sqrt{p(t)}} \left(\cos \frac{\theta}{2} |0\rangle + e^{i\phi} \sin \frac{\theta}{2} f_{1,N}(t) |1\rangle \right) \quad (7)$$

with

$$p(t) = \cos^2 \frac{\theta}{2} + |f_{1,N}|^2 \sin^2 \frac{\theta}{2} \quad (8)$$

and

$$f_{1,N} = \langle N | e^{-iHt} | 1 \rangle \quad (9)$$

is the transition amplitude of the excitation over the array. As the state to be transmitted is unknown, we will average the fidelity of the quantum communication over the whole Bloch sphere to characterize the quality of the chain as a transferring media

$$F(t) = \frac{1}{4\pi} \int \langle \psi_{in} | \rho_{out} | \psi_{in} \rangle d\Omega . \quad (10)$$

After integration we get an explicit formula [8]

$$F(t) = \frac{1}{2} + \frac{|f_{1,N}(t)| \cos \gamma}{3} + \frac{|f_{1,N}|^2(t)}{6} \quad (11)$$

with

$$\gamma = \arg f_{1,N} \quad (12)$$

Equation (11) is one of the main results in [8] and it is valid for all Hamiltonians that conserve the number of excitations in the chain.

Up to now it is not clear why the averaged fidelity should be the quantity that we are interested in while studying the state transfer over the chain. The more intuitive measure of the transmission quality is the minimal fidelity given by

$$F_m = \min_{\psi_{in}} \langle \psi_{in} | \rho_{out} | \psi_{in} \rangle \quad (13)$$

We will now show that both measures F and F_m are equivalent. It means that if some chain is worse than another chain in terms of one measure it will be worse in terms of another measure as well and a maximum of F corresponds to a maximum of F_m . Indeed, for the fidelity of a given state $|\psi_{in}\rangle = \cos(\theta/2)|0\rangle + e^{i\varphi} \sin(\theta/2)|1\rangle$ we can write an expression

$$F(\theta, \phi) = (1 - p(t)) \cos^2 \frac{\theta}{2} + \left(\cos^2 \frac{\theta}{2} + f_{1,N}^* \sin^2 \frac{\theta}{2} \right) \left(\cos^2 \frac{\theta}{2} + f_{1,N} \sin^2 \frac{\theta}{2} \right) \quad (14)$$

or explicitly writing $p(t)$ after some trigonometric transformations

$$F(\theta, \phi) = \frac{1 + \cos \theta}{2} - |f_{1,N}|^2 \frac{1 - \cos \theta}{2} \cos \theta + \frac{f_{1,N}^* + f_{1,N}}{4} \sin^2 \theta \quad (15)$$

in the case $f_{1,N}^N(t) \equiv f = |f|$ we can write it as

$$F(\theta, \varphi) = \frac{1 + f}{2} + \cos(\theta) \frac{1 - f^2}{2} + \cos^2(\theta) \frac{f^2 - f}{2}. \quad (16)$$

The function changes monotonically from 1 for the $|0\rangle$ state to $F_m = f^2$ for the $|1\rangle$ state. One can easily see that in this case the maximum of F_m is achieved when f is maximal, that also corresponds to the maximum of the averaged fidelity $F = 0.5 + f/3 + f^2/6$. However, while both fidelities are monotonic functions of f , their difference $\delta F = |F_m - F| = 0.5 + f/3 - 5f^2/6$ is not monotonic and has a maximum at $f = 0.2$.

For $f \neq |f|$ the fidelity can have a local minimum for $\theta \neq \pi$. Since $F(\theta, \phi)$ turns to be independent of ϕ , we can easily find this minimum by taking the derivative over θ . Using the fact that $f_{1,N}^* + f_{1,N} = 2|f_{1,N}| \cos \gamma$ we have

$$F'(\theta, \phi) = -\frac{1}{2} \sin \theta \left[1 - |f_{1,N}|^2 + 2 \cos \theta (|f_{1,N}|^2 - |f_{1,N}| \cos \gamma) \right] \quad (17)$$

From (17) we get

$$F'(\theta, \phi) = 0 \Rightarrow \begin{cases} \theta = 0 \\ \theta = \pi \\ 1 - |f_{1,N}|^2 = 2 \cos \theta (|f_{1,N}|^2 - |f_{1,N}| \cos \gamma) \end{cases}$$

The first two solutions correspond to a maximum/minimum at the ends of the considered interval $\theta \in [0, \pi]$. The third solution is valid when $|f| > \cos(\gamma)/3 + \sqrt{\cos^2(\gamma) + 3}/3$. In this case there is a local minima at $\theta = \arccos\left(\frac{1-|f|^2}{2(|f|\cos(\gamma)-|f|^2)}\right)$, but this minimum is maximal when γ is a multiple of 2π . Therefore, if we want to maximize F_m , we will have $\cos(\gamma) = 1$ which leads again to Eq. 16. This proves that we can safely use the average fidelity as a quantity that characterizes the quality of the state transfer and compare different chains and protocols by comparing averaged fidelities.

1.3 Heisenberg Hamiltonian

A particular example of a Hamiltonian that conserves the number of excitations was proposed in [8]. It is a Hamiltonian that describes a linear chain of N spins coupled by an isotropic Heisenberg interaction in the presence of magnetic field

$$H = -\frac{J}{2} \sum_{i=2}^N (\sigma_i^x \sigma_{i-1}^x + \sigma_i^y \sigma_{i-1}^y + \sigma_i^z \sigma_{i-1}^z) - \sum_{i=1}^N B \sigma_i^z. \quad (18)$$

It was analytically solved in [8] and its eigenenergies and eigenstates are

$$E_n = 2B + 2J \left(1 - \cos \frac{\pi(n-1)}{N} \right), \quad (19)$$

$$|\tilde{n}\rangle = \sqrt{\frac{1+\delta_{n1}}{N}} \sum_k \cos\left(\frac{\pi(n-1)}{2N}(2k-1)\right) |k\rangle, \quad (20)$$

for

$$n = 1, \dots, N .$$

We can express the transition amplitude using (19) and (20) as

$$f_{1,N}(t) = \sum_{n=1}^N \langle 1|\tilde{n}\rangle \langle \tilde{n}|N\rangle e^{-iE_n t} , \quad (21)$$

that leads us to

$$f_{1,N}(t) = \sum_{n=1}^N \frac{1 + \delta_{n1}}{N} \cos \frac{\pi(n-1)}{2N} \cos \left(\frac{\pi(n-1)}{2N} (2N-1) \right) e^{-iE_n t} , \quad (22)$$

and using

$$\cos \left(\pi(n-1) - \frac{\pi(n-1)}{2N} \right) = (-1)^n \cos \frac{\pi(n-1)}{2N} , \quad (23)$$

we get

$$f_{1,N}(t) = \sum_{n=1}^N \frac{1 + \delta_{n1}}{N} (-1)^n \cos \left(\frac{\pi(n-1)}{2N} \right)^2 e^{-i[2B+2J(1-\cos \frac{\pi(n-1)}{N})]t} . \quad (24)$$

Using equation (24) one can easily evaluate $f_{1,N}$ and therefore the averaged fidelity F even for long chains, see Fig. 1. We would like to mention, that by varying the magnetic field B we can change the phase of the complex quantity $f_{1,N}$ and thus make γ a multiple of 2π at any given time to maximize the averaged fidelity (11).

1.4 Improved quantum state transfer in spin chains

It was shown [8] that for short-length chains the fidelity of the state transfer is high, i.e., close to one and is higher than the maximal fidelity of the state transfer realized only by classical communication ($2/3$ according to [9]). However, the fact that it is substantially reduced with the length of the chain, see Fig. 1, triggered the search of methods that allow to increase the fidelity or even to obtain perfect state transfer,

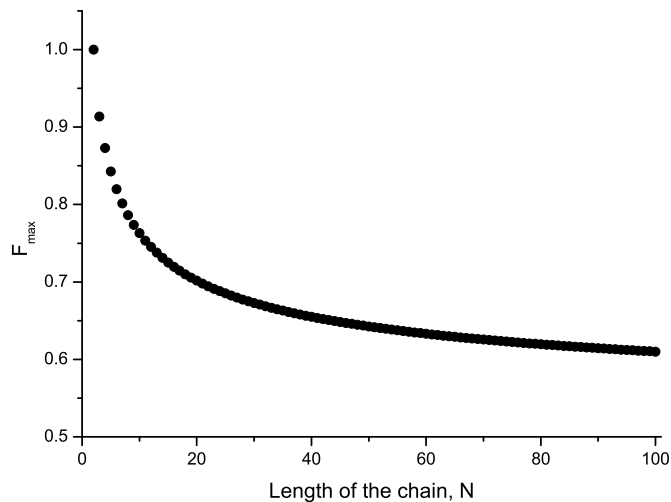


Figure 1: The first maximum of the averaged fidelity $F(t)$ as a function of a chain length.

in the absence of decoherence and relaxation processes. It is achieved when receiver recovers an input state on the last spin, while sender normally loses his state, in fulfillment of the no-cloning theorem [10]. In fact, we would like to achieve the ideal state transfer under the assumption that quantum error correction algorithms can be used, that gives us a threshold for the fidelity value $1 - 3\%$ [11].

The main reason for imperfect transfer is the dispersion of the initial information over the whole chain. Most of the proposals that realize improved state transfer minimize this dispersion in one or another way.

One of the more intuitive ways to improve the fidelity is to use spatially varying coupling constants to “refocus” the information at the receiving part of the chain [12, 13, 14]. These methods do not require extra resources or extra control. The idea is to adjust the coupling between the spins in such a way, that the ratios of the eigenenergies of the Hamiltonian are rational numbers. One of the particular forms of the Hamiltonian, proposed independently in [12] and [15] is

$$H_0 = -J_{xy} \sum_{n=1}^{N-1} \sqrt{n(N-n)} (\sigma_n^x \sigma_{n+1}^x + \sigma_n^y \sigma_{n+1}^y) , \quad (25)$$

then the evolution operator

$$U(t) = \exp(-iH_0 t) , \quad (26)$$

describes the rotation of a spin $\frac{1}{2}(N-1)$ particle and the transition amplitude of the excitation over the spin chain is

$$f_{1,N}(t) = (-i \sin 2J_{xy} t)^{(N-1)} . \quad (27)$$

Thus, a state transfer with $|f_{1,N}| = 1$ can be realized for the time

$$t = \frac{\pi + 2\pi n}{4J_{xy}} . \quad (28)$$

If we add a magnetic field to the Hamiltonian

$$H = H_0 + \sum_{i=1}^N B \sigma_i^z \quad (29)$$

we can achieve the perfect state transfer by choosing B in such a way that

$$\arg f_{1,N} = 2\pi . \quad (30)$$

There are also other proposals to achieve perfect or nearly perfect state transfer using engineered coupling constants [16, 17, 18].

The idea of the so-called conclusive transfer, providing perfect state transfer using parallel quantum channels [19, 20], see Fig. 2, is very promising. It can be realized using almost any spin chain and it is stable against fluctuations of the chain parameters [21]. The state is encoded as a superposition of the excitations in both chains

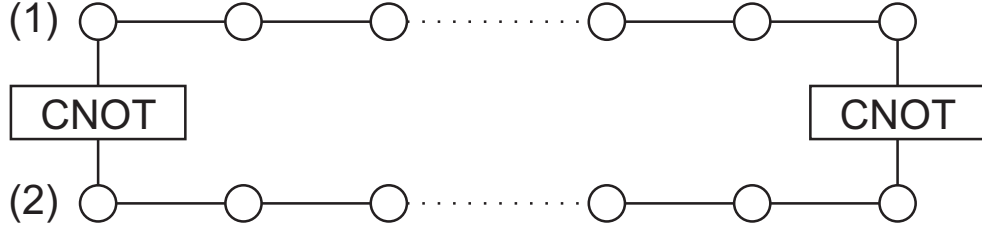


Figure 2: Schematic of dual raid encoding.

by initializing the first qubit of chain the (1) in the state to be transmitted and then applying a CNOT gate to the first qubit of the chain (2) with the first qubit of the chain (1) as a control qubit. After some specific time, namely when the absolute values of the transmission amplitudes of the excitation over the arrays are equal for both chains $|f_{1,N}^1(t)| = |f_{1,N}^2(t)|$, the receiver applies a CNOT gate at his part of the chain. After that, he performs a measurement on his qubit in the chain (2). If the result of the measurement is the excited state (that happens with probability $|f_{1,N}^1(t)|^2$), then the last qubit in the chain (1) contains the state to be transmitted. If the outcome is a ground state, the protocol can be repeated till the receiver gets the state, under assumption that there are no relaxation and decoherence processes in the system. The basic intuitive explanation why perfect state transfer can be achieved is that by applying the CNOT gate, we introduce the dispersion of the state $|0\rangle$. If we then apply a CNOT gate at the receiver part of the chain at the time when $|f_{1,N}^1(t)| = |f_{1,N}^2(t)|$ and measure the excitation in the second chain, then we will get simply an amplitude damping channel for the state $\phi = \cos \frac{\theta}{2}|0\rangle + e^{i\phi} \sin \frac{\theta}{2}|1\rangle$. The imperfection of the single chain transfer is now manifested not in the fact that fidelity is smaller than unity, but in the fact that probability of measuring the desired state is not unity. And since we don't get any information about the state if the measurement is failed, this information is still contained in the chain and can be obtained in the next measurements.

Another possibility to get ideal or near-ideal state transfer is to encode the in-

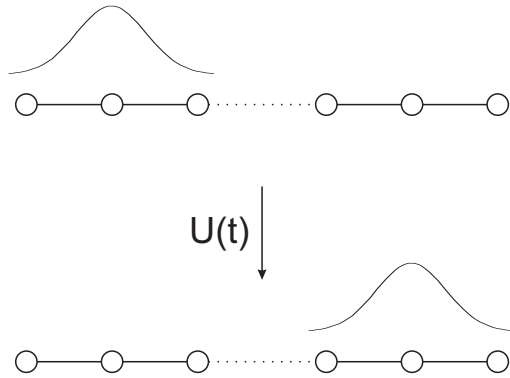


Figure 3: Schematic of Gaussian wave-packet encoding.

formation in Gaussian wave packets (with low dispersion) spread over several spins [22], see Fig 3. In this case both the sender and the receiver should control parts of the chain instead of one qubit. The longer is the part of the chain controlled by the sender, the longer should be the part controlled by the receiver. The sender has to encode the state to be transmitted in a Gaussian-modulated superposition of qubits in his part of the chain. The receiver then has to decode this information in his part of the chain.

Instead of coding information using several neighbor qubits in one chain, one can do it by using only the first qubits of several chains [23]. It was shown that using an optimal coding/decoding strategy asymptotically allows to achieve perfect state transfer *and* optimal efficiency.

One can also achieve high fidelity of the state transfer by using chains where the first and last qubits are only weakly coupled to the rest of the chain [24, 25]. The reason for nearly perfect transfer is that the intermediate spins are only slightly excited, which means that dispersion is small. Actually, one can achieve arbitrary high fidelity by making the coupling strength smaller. This method has the major disadvantage that the time required for the transfer is long compared to the qubit decoherence/relaxation times in present experimental setups. To achieve a fidelity as big as $1 - \delta$ for chains of odd length N , the time of the state transfer will be of the

order of $\frac{2N/\pi}{\sqrt{\delta}}$ [24].

Another proposal that exploits the same gapped system behavior when intermediate spins are only slightly excited and therefore dispersion is small was investigated in [26].

Finally, we have to mention that use of time-dependent control of some parameters of the Hamiltonian can improve the fidelity of the quantum state transfer. Time-dependent gates between each pair of qubits, for example swap gates that can be switched on and off, will build a perfect transmission line, but are hard to realize. It also is, in general, superfluous if we want to achieve good fidelity (~ 0.99) and use quantum error correction to repair the state. In fact, in practice each gate will introduce an error and using many non-ideal gates can significantly reduce the fidelity for relatively long chains. While use of static coupling constants with time-dependent control of some parameters of the Hamiltonian allows us to perform perfect or nearly perfect state transfer. It was shown in [27] that if the coupling at the end of the chain can be controlled arbitrary then the Gaussian wave packet encoding scheme [22] can be simulated. Another possibility is to use some global fields, for example pulsed global rotations [28, 29, 30].

1.5 Outline

This thesis is organized as follows. Chapter 2 describes different schemes for coupling two superconducting qubits, focussing on variable coupling schemes, that allow to realize two-qubit gates which are necessary to build a universal set of quantum gates. Chapter 3 is devoted to one particular scheme of charge qubit sign-tunable coupling. In Chapter 4 we discuss the quantum state transfer in arrays of flux qubits. Chapter 5 is devoted to the use of dynamical coupling between just two pairs of qubits in the chain for improved quantum state transfer. Finally, in Chapter 6 we discuss the role of quantum interference in the state transfer via spin chains.

2 Coupling of two superconducting qubits

2.1 Introduction

According to the 4th DiVincenzo criteria, a universal set of quantum gates is required for implementation of quantum computation. While single qubit operations are relatively easy to perform [31, 32, 33], controllable coupling of two qubits is still a challenge. Such interaction is also an essential part of time-dependent control required for improved quantum state transfer described in Chapter 5 of this thesis. In this chapter we will describe and classify different proposals and technics that allow to achieve controllable inter-qubit coupling for superconducting charge and flux qubits. In this classification we will distinguish between tunability of the coupling (ability to change coupling constant) and sign-tunability of the coupling. Sign-tunability means that the coupling could change its sign and, therefore, it can be switched off. The ability to change the sign of the coupling and switch it off completely is useful for several applications, see for example Chapter 5. But in general it is not required for building a universal set of quantum gates.

In this chapter we will consider only two types of superconducting qubits: the charge qubit represented by the Cooper-pair box and the flux qubit represented by a loop with three small-capacitance Josephson junctions (so-called Delft design). This is done only to simplify the presentation of the methods that allow us to couple two qubits. Other types of qubits based on the charge and flux degrees of freedom can also be coupled using these methods. The flux qubit design is discussed in detail in Chapter 4, while the Cooper-pair box is simply a small superconducting island with n excess Cooper-pairs, connected by a tunnel junction with capacitance C_J and Josephson coupling energy E_J to a superconducting electrode, see Fig. 4. We will assume that our systems are in qubit regime with Hamiltonian

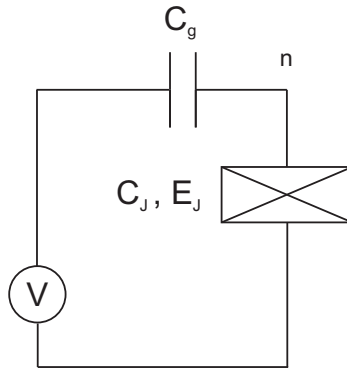


Figure 4: Simplest charge qubit.

$$H = -B\sigma^z + \Delta\sigma^x \quad (31)$$

where σ^z , σ^x are Pauli matrices and B , Δ are some constants.

2.2 Static coupling between qubits

Conceptually, the simplest type of coupling between qubits is direct static coupling. For example one can couple two Cooper-pair boxes via a capacitor [34, 35] or fabricate two flux qubits close to each other so they would have a small inductive coupling between each other [36, 37], see Fig. 5 (a),(b). The resulting charge-charge or flux-flux interaction is described by the Ising-type coupling term

$$H_{coupl} \propto \sigma_1^z \sigma_2^z . \quad (32)$$

Despite its simplicity and absence of tunability one can perform two-qubit gates based on static coupling using special protocols described later in this section.

We would like to mention, that the numerical value of the inductive coupling constant estimated for conducting loops of actual qubits is very small. It turns out to be at least one order of magnitude smaller than typical values of the constants B and Δ [38]. Therefore it was proposed to use shared big Josephson junction to

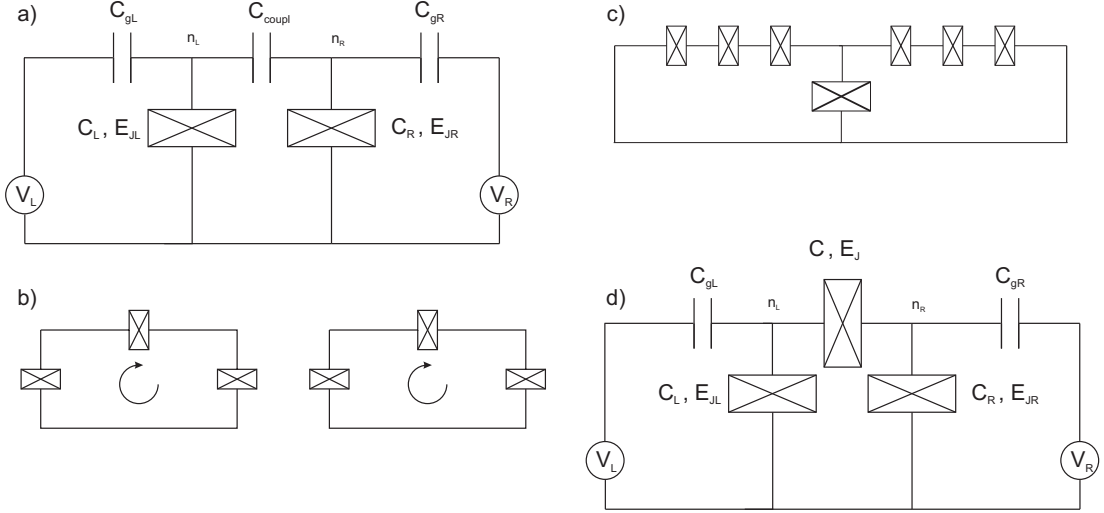


Figure 5: Simple static coupling between the two qubits. (a) Two Cooper-pair boxes connected by a capacitor. (b) Two flux qubits located near each other, coupled by the magnetic flux that one qubit induce in the other nearby qubit. (c) Two flux qubits coupled by a shared Josephson junction. (d) Two charge qubits coupled by a Josephson junction.

increase the coupling strength [38], see Fig. 5 (c). In the regime when the Josephson energy of the shared junction J_S is much bigger than the Josephson energy of the loop junctions J , the phase drop across large junction is much smaller than the overall phase change. Therefore coupling do not perturb the dynamics of individual qubits. However, the coupling strength is of the order of J^2/J_S and can be made comparable to the parameters B and Δ .

Instead of coupling two flux qubits by their mutual inductance, one can use a common loop inductance, as proposed in [39]. This is shown in Fig. 6.

The main advantage of this proposal is that a strong interqubit coupling can be achieved using a small inductance, so that two-bit operations as fast as one-bit ones can be easily realized.

If we would replace the capacitor between two charge qubits by a Josephson junction, the Cooper-pairs could tunnel between the left and the right superconducting islands. This will correspond to the extra term in the Hamiltonian [40]

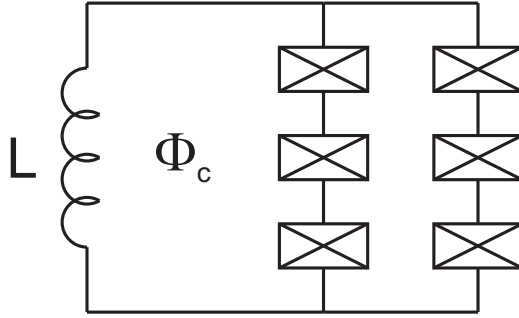


Figure 6: Two flux qubits coupled by common inductance, after [39].

$$H_{coupl} \propto \sigma_1^+ \sigma_2^- + \sigma_1^- \sigma_2^+ , \quad (33)$$

where $\sigma^+ = \sigma^x + i\sigma^y$ and $\sigma^- = \sigma^x - i\sigma^y$. Since a Josephson tunnel junction has some capacitance, there always would be small Ising-type coupling term presented in a coupling Hamiltonian. One can achieve similar coupling between the flux qubits, that allows them to exchange the excitations, by coupling them via a capacitor [38], see Fig. 7 (a). More detailed explanation why such coupling provides Hamiltonian of a form (33) can be found in Chapter 4. One could also achieve coupling described by Hamiltonian

$$H_{coupl} \propto \sigma_1^+ \sigma_2^+ + \sigma_1^- \sigma_2^- , \quad (34)$$

by using modified coupling via capacitor, see Fig. 7 (b).

By comparing coupling Hamiltonians (32) and (33) with Heisenberg Hamiltonian (18), we see that the static coupling schemes described above allow us to realize quantum state transfer in the chains of charge/flux qubits. Also we have to mention, that despite being useful in the realization of quantum state transfer, capacitive coupling between flux qubits has the disadvantage that it introduces sensitivity to offset charges. The inductive and shared junction couplings ($\propto \sigma^z \sigma^z$) do not have this problem.

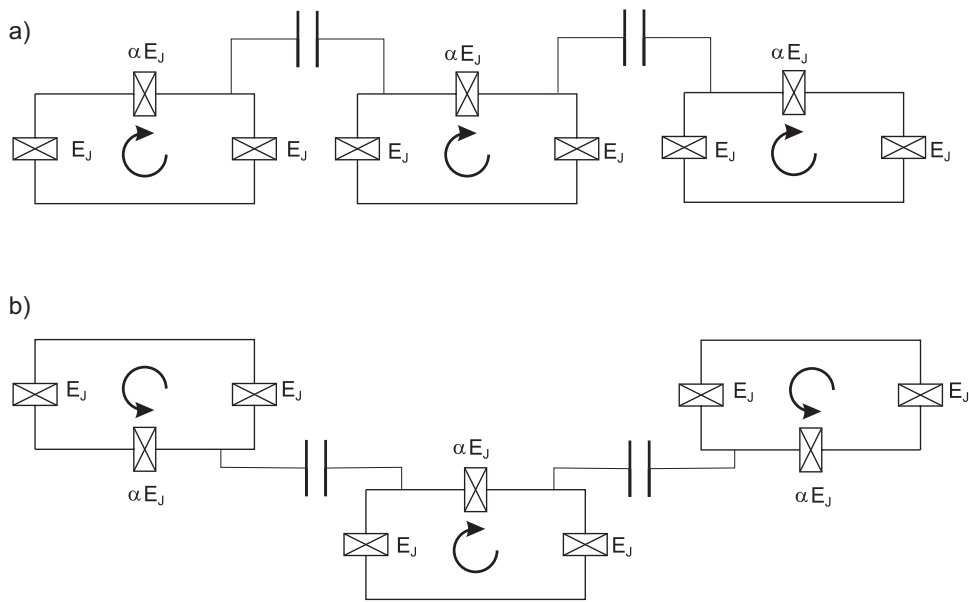


Figure 7: Two flux qubits coupled via capacitor after [38]. (a) Realization of transverse inter-qubit coupling described by Hamiltonian (33). (b) Realization of transverse inter-qubit coupling described by Hamiltonian (34).

2.2.1 Techniques to realize two qubit gates with static coupling between qubits

Even if the coupling constants can not be controlled in static coupling schemes, one can perform universal gates by using special experimental protocols. Here we describe several proposals how to do so. From a practical point of view, we would like to have our charge/flux qubits biased at a symmetry point [41, 42] (the so called *optimal point*) where their coherence times are the longest because they are insensitive to the first order to the main noise source (charge and flux-noise respectively). Generally the static coupling at the optimal point fails due to the energy mismatch, as even a small deviation in parameters of the two qubits will result in different energy gaps. Two coupled qubits can exchange energy only if they are on resonance. This is another reason why we need some special protocols to couple two qubits, if we want them to be biased in their optimal points. We will present only two such protocols, though another realizations of similar ideas are possible.

FLICFORQ protocol

The FLICFORQ protocol (fixed linear couplings between fixed off-resonant qubits) was proposed in [43]. The idea is to use qubits with fixed, detuned Larmor frequencies and fixed coupling strengths ($\sigma^z\sigma^z$ coupling). By simultaneously irradiating two qubits at their respective Larmor frequencies with appropriate amplitude and phase one can achieve two-qubit gates. The essence of the method is similar to the techniques used in NMR quantum computing. Qubit-photon coupling creates dressed states and by matching the frequencies two qubits could exchange photons through coupling reactance. The Hamiltonian of the irradiated qubits is [43]

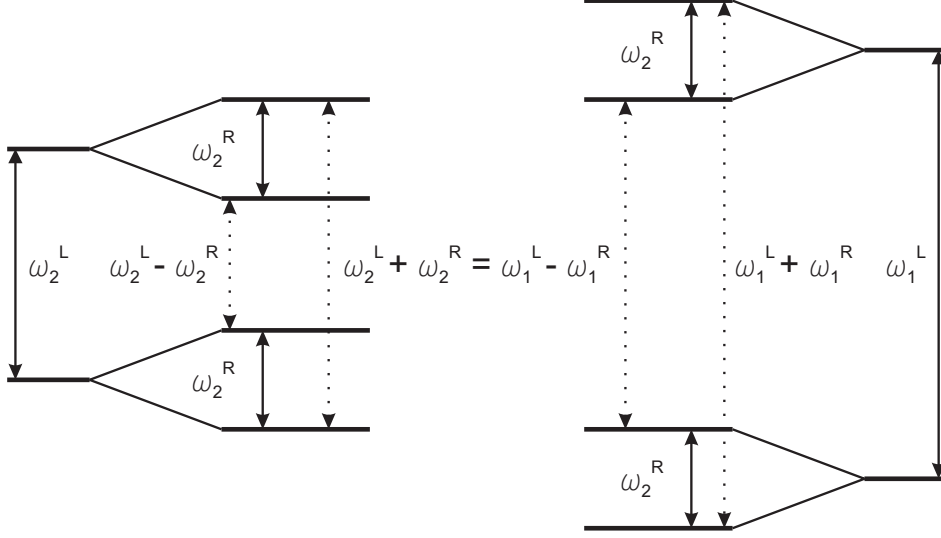


Figure 8: Dressed states energy diagram after [43].

$$\frac{H}{\hbar} = \frac{1}{2}\omega_1^L\sigma_1^z + \frac{1}{2}\omega_1^R \cos(\omega_1^{rf}t + \phi_1)\sigma_1^x + \frac{1}{2}\omega_2^L\sigma_2^z + \frac{1}{2}\omega_2^R \cos(\omega_2^{rf}t + \phi_2)\sigma_2^x + \frac{1}{2}\omega^{xx}\sigma_1^x\sigma_2^x \quad (35)$$

were $\omega_a^L/2\pi$ is the Larmor frequency of qubit a , ω_a^R and $\omega_a^{rf}/2\pi$ are, respectively, the amplitude and frequency of the signal applied to qubit a , and $\omega^{xx}/2\pi$ is the entangling frequency. The mechanism allowing very weak nonsecular interqubit coupling ω^{xx} is easily understood in the dressed atom picture of quantum optics, see Fig 8. Two dressed qubits may absorb and emit energy at frequencies $\omega_1^L \pm \omega_1^R$ and $\omega_2^L \pm \omega_2^R$, respectively. Choosing $\omega_1^L - \omega_2^L = \omega_1^R + \omega_2^R$ causes the upper sideband of qubit 1 to overlap the lower sideband of qubit 2. Therefore qubits can exchange photons of the energy $\hbar(\omega_1^L - \omega_2^L) = \hbar(\omega_1^R + \omega_2^R)$ through the coupling reactance.

It was shown in [43] that one can perform two-qubit $\pi/2$ rotation $(Y_1Y_2)^{1/2} = (1 + \sigma_1^y\sigma_2^y)/\sqrt{2}$. Together with single-qubit gates (performed by single-qubit irradi-

ation pulses) it builds an universal set for quantum computation. The advantage of this technique is the fact that qubits may stay in their optimal bias point where the first order decoherence to fluctuations in control parameters is suppressed.

Controllable coupling between flux qubits using time-dependent magnetic flux

A slightly different protocol was proposed in [44] to couple two flux qubits using time-dependent magnetic flux (TDMF). The qubits are assumed to be placed near each other and to interact through a mutual inductance, see Fig. 5 (b). Two-qubit coupling and decoupling are controlled only by *the frequency* of the applied TDMF. Therefore the bias magnetic flux is not changed. The controllable coupling is realized, when the large detuning condition is satisfied. Then in the absence of TDMF qubits can be approximately treated as two decoupled subsystems. To couple two qubits with assistance of the TDMF one has to [44]

- apply TDMF through one of the qubits, and its frequency should be equal to detuning (or sum) of the two-qubit frequencies
- the reduced bias flux [45] on the qubit, which is addressed by TDMF, should be near but not equal to 1/2.

The last condition shifts the qubit from the optimal point thus making the decoherence time short. However this proposal can work for small deviation from optimal point and therefore can be realized in practice to couple two superconducting flux qubits. In [44] it was shown that using TDMF one can realize two Hamiltonians

$$H_1 \propto \sigma_1^+ \sigma_2^- + H.c. , \quad (36)$$

and

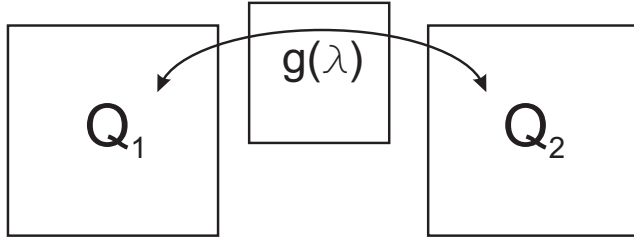


Figure 9: Parametric coupling scheme: two qubits coupled through a circuit that allows to modulate the coupling constant g through the control parameter λ , after [46].

$$H_2 \propto \sigma_1^+ \sigma_2^+ + H.c. . \quad (37)$$

Using the Hamiltonians H_1 and H_2 one can implement any two-qubit gate and together with single qubit operations get an universal set for quantum computation.

2.3 Parametric coupling for superconducting qubits

Another way to couple detuned qubits biased at their optimal point was proposed in [46]. The disadvantage of the FLICFORQ protocol is the fact that to satisfy the resonance condition, the two qubits should be reasonable close in energy. Otherwise large driving of each qubit could potentially excite higher energy states or uncontrolled environmental degrees of freedom [46].

Parametric coupling relies on the possibility to control a coupling constant between two qubits by a control parameter λ , see Fig. 9.

By modulating λ at the frequency close to the detuning (or sum) of the qubit frequencies, one can achieve a controllable coupling between the qubits. The difference between parametric coupling and the scheme proposed in [44] is that by modulating the coupling between the qubits instead of applying the flux pulses directly through the qubits allows qubits to stay in their optimal point.

Parametric coupling scheme require some tunable circuit that couple two qubits.

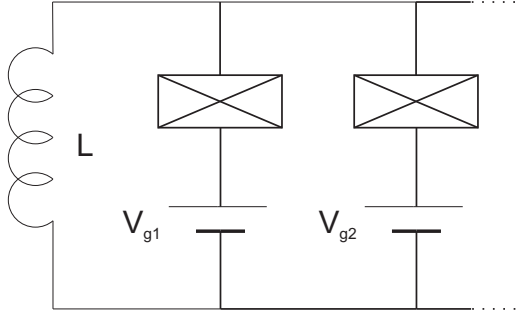


Figure 10: LC circuit formed by inductance and the qubit capacitors, after [47].

In the rest of this chapter we will describe such circuits for flux and charge qubits. Note, that not all schemes realize a controllable $\sigma^z\sigma^z$ interaction required for parametric coupling. But other types of controllable interactions like $\sigma^y\sigma^y$, $\sigma^x\sigma^x, \sigma^+\sigma^- + H.c.$ also allow us to build a universal set of quantum gates required for quantum computing

2.4 Dynamical coupling between qubits using additional circuits

2.4.1 Circuits to couple charge qubits

Several schemes were proposed to achieve controllable charge qubit coupling using additional circuits and circuit elements. To our knowledge, the first scheme was proposed in [47]. It is shown in Fig. 10.

All qubits are connected in parallel to a common LC-oscillator mode. It was shown in [47] that this scheme realizes coupling Hamiltonian

$$H_{coupl} = - \sum_{i < j} g_{ij} \sigma_i^y \sigma_j^y + const \quad (38)$$

the coupling constant g_{ij} depends on the inductance L and Josephson energies of the qubit tunnel junctions. Therefore, if the single Josephson junction in each qubit

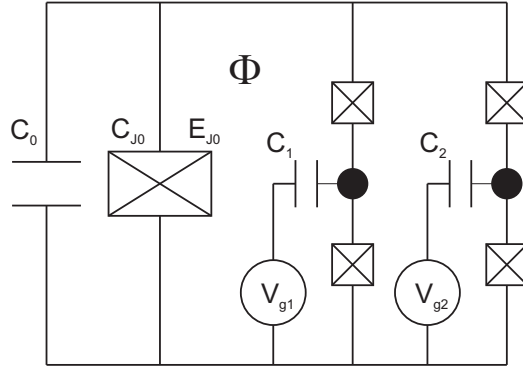


Figure 11: Two charge qubits coupled by a large Josephson junction, after [49]. Each filled circle denotes a superconducting island, which is biased by a voltage V_{g_i} via the gate capacitance C_i and coupled to the bulk superconductors by two identical small Josephson junctions

is replaced by a SQUID (to achieve controllable E_J) the coupling can be controlled by fluxes through the SQUID loop.

The drawback of this type of coupling is that the eigenfrequency ω_{LC} of the LC circuit is much higher than the quantum manipulation frequencies. Therefore there is a *limit* for allowed number N of the qubits in the circuit because ω_{LC} scales with $1/\sqrt{N}$.

Another way to achieve controllable coupling between charge qubits is to replace the Josephson junction in Fig. 5 (d) by a SQUID to control the tunneling rate of the Cooper-pairs [48]. Then the coupling will be described by the Hamiltonian

$$H_{coupl} = -g(\Phi)\sigma_1^+\sigma_2^- + H.c. \quad (39)$$

where Φ is the magnetic flux through the SQUID loop.

Instead of using a large Josephson junction (or SQUID) between two qubits, one can arrange it parallel to achieve coupling as described in [49], see Fig. 11.

To ignore the large Josephson junction capacitance, a large capacitance C_0 is placed in a parallel with it. Then the flux quantization around loops containing the

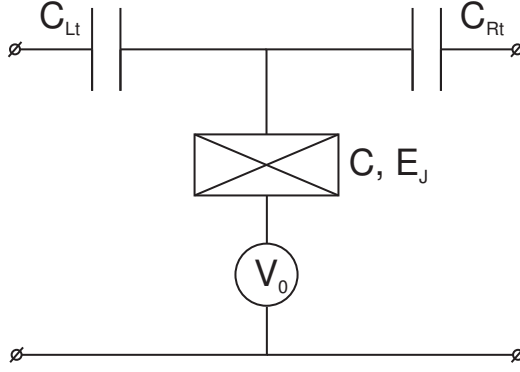


Figure 12: Variable electrostatic transformer, after [50].

phase drops of involving junctions leads to the effective interaction Hamiltonian

$$H_{coupl} = g(\Phi)\sigma_1^x\sigma_2^x \quad (40)$$

where Φ is applied flux. It was also shown in [49] that replacing the large Josephson junction by a symmetric dc SQUID with two sufficiently large junctions one can implement both controllable $\sigma_1^x\sigma_2^x$ -coupling and the readout.

A variable electrostatic transformer was proposed in [50] to achieve controllable $\sigma_1^z\sigma_2^z$ coupling between two charge qubits. The scheme is shown in Fig. 12. A small Josephson junction confined in its lowest energy band behaves as a variable capacitance with respect to the injected charge [51]. This scheme will be discussed in detail in Chapter 3.

Another proposal, that utilizes a large Josephson junction to create a controllable coupling between charge qubits was proposed in [52]. The qubits are represented by Single Cooper Pair Transistors with loop-shaped electrodes coupled together by current biased coupling Josephson junction at the loop intersection, see Fig. 13.

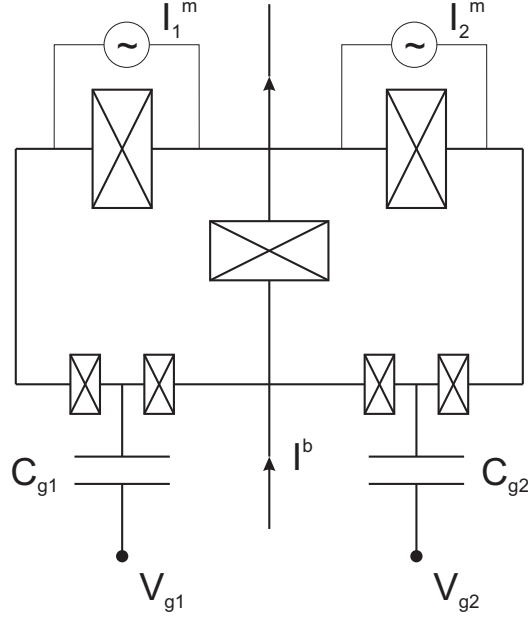


Figure 13: Single Cooper Pair Transistors coupled by large Josephson junctions, after [52]. Single-qubit readout can be performed by applying a current I^m to a particular readout junction. The interaction of the qubits is controlled by the qubit bias I^b or by simultaneous current biasing of readout junctions.

Left without any external biasing of the coupling two charge qubits are independent neglecting a weak residual interaction. By applying a non zero current bias I^b or by simultaneously applying dc bias currents I_i^m to both readout junctions one can achieve the coupling described by the Hamiltonian

$$H_{coupl} = g(I^b, \phi_1, \phi_2) \sigma_1^x \sigma_2^x \quad (41)$$

where ϕ_1 and ϕ_2 are phase drops across the readout junctions. A small residual coupling prevents us from switching the interaction off completely, but the ability to modulate the coupling strength together with the ability to perform single-qubit operations is enough to build a universal set of quantum gates.

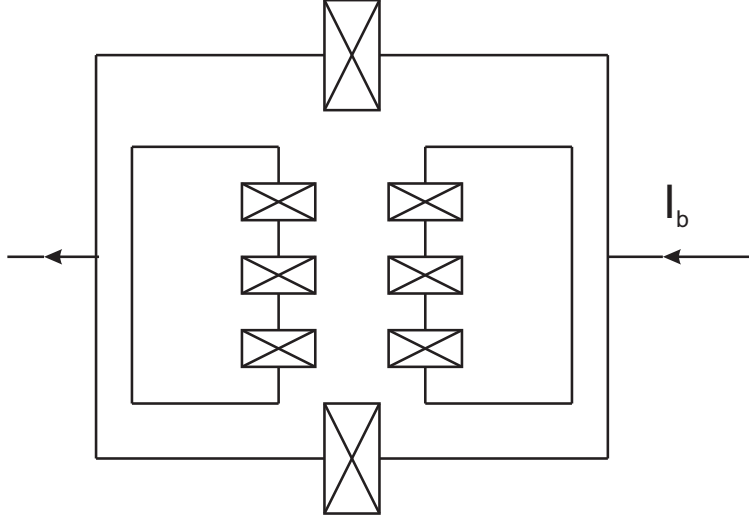


Figure 14: SQUID-based coupling scheme, after [53]. The coupling is mediated by a bias current I_b

2.4.2 Circuits to couple flux qubits

The simplest idea, utilized in most proposals mentioned here, is to use an extra loop/circuit that is galvanically coupled to both qubits to create a controllable interqubit coupling. Quite often the same circuit can be used to read out the flux states of the qubits.

It was shown in [53], that one can achieve tunable coupling by placing two qubits near the same dc SQUID, see Fig. 14. Each qubit is coupled to the SQUID loop through a mutual inductance and thus coupled to each other indirectly. SQUID bias current I_b can be used to control the coupling strength g in a coupling Hamiltonian

$$H_{coupl} = g(I^b)\sigma_1^z\sigma_2^z \quad (42)$$

This coupling is sign-tunable (thus switchable) [53, 54]. By applying pulses of bias current one can perform the CNOT operation that is sufficient to build a universal set of quantum gates.

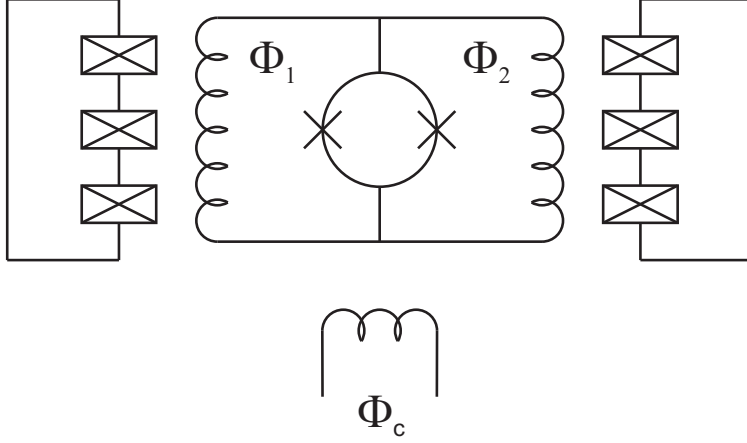


Figure 15: Variable inductance transformer scheme, after [55]. The qubits are coupled to two branches of the device via fluxes Φ_1 and Φ_2 . The control is achieved by a control flux Φ_c .

The idea to use variable inductance transformer, equivalent to variable capacitance transformer [50], to couple two flux qubits or to couple one flux qubit to read out SQUID was proposed in [55]. The scheme is shown in Fig. 15. Each qubit is coupled by mutual inductance to one of the branches of the transformer and control flux Φ_c can be used to vary the coupling strength g in a coupling Hamiltonian

$$H_{coupl} = g(\Phi^c)\sigma_1^z\sigma_2^z \quad (43)$$

This scheme also allows to create a bus to couple multiple qubits with each other [56].

Niskanen *et al.* proposed to use a high-frequency qubit placed between two flux qubits and coupled to them via mutual inductance for parametric coupling scheme described above [57]. The circuit used can be identical to the primary qubits, but the splitting should be larger so that the third (coupling) qubit is always in the ground state. There is an optimal point in the coupling energy, where it is insensitive to a

low-frequency flux noise, therefore making the experimental realization easier.

There are also other proposals, not described here, that could be used to create a tunable coupling between two qubits, see for example [58, 59, 60] and citations in papers mentioned in this chapter. One can also use variable capacitance schemes to create controllable ($\sigma^+\sigma^- + H.c.$) between the flux qubits and replace Josephson junction/SQUID with variable inductance schemes for charge qubits.

2.5 Conclusion

In this chapter a number of proposals for coupling two superconducting qubits were discussed. We have seen that there are different ways to realize a two qubit gate that together with single qubit gates will build a universal set of quantum gates for quantum computation.

3 Variable coupling scheme for superconducting charge qubits

3.1 Introduction

In this chapter we will analyze more closely the circuit, that implements a controllable coupling of charge qubits [50], see Fig. 12. It was proposed as a generalization of a simple capacitive coupling. The authors of this proposal use the fact, that a small Josephson junction confined in its lowest energy band behaves as a variable capacitance with respect to the injected charge [51]. One of the most important features of this scheme is a sign-tunability of this capacitance. It implies the possibility to switch the coupling on and off. For more details look at the original paper [50]. Here we will shortly present the approximation, that was used to obtain analytical results and then check the range of validity for this approximation using numerical calculations. We will also analyze the influence of E_{J_i} on the lowest energy band of the system.

3.2 Born-Oppenheimer-like approximation

If we insert the transformer Fig. 12 between the two charge qubits Fig. 16, the Hamiltonian of the system can be written as follows:

$$H = - \sum_{i=L,R} [E_{J_i} \cos \phi_i + E_{C_i}(n_i - q_i)^2] - E_J \cos \phi + E_C [n - q(n_L, n_R)]^2 \quad (44)$$

where

$$E_C = \frac{2e^2}{C + C_{tR} + C_{tL} - C_{tR}^2/(C_R + C_{gR} + C_{tR}) - C_{tL}^2/(C_L + C_{gL} + C_{tL})} \quad (45)$$

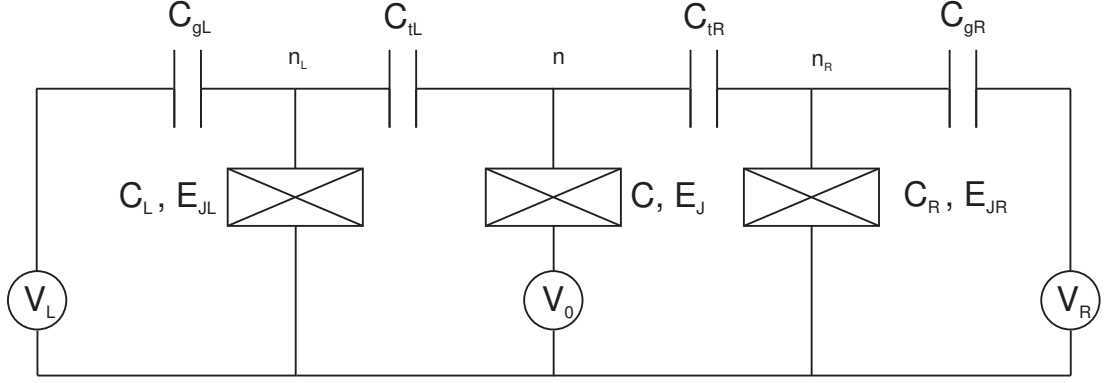


Figure 16: Two qubits coupled by a variable electrostatic transformer.

$$E_{Ci} = \frac{2e^2}{C_i + C_{gi} + C_{ti}} \quad (46)$$

$$q_i = \frac{V_i C_{gi}}{2e}. \quad (47)$$

Here n_i is the number of excess Cooper pairs on qubit i , $q(n_L, n_R)$ is the charge induced on the transformer junction defined by

$$q = q_0 - \sum_{i=L,R} \frac{(n_i - q_i) C_{ti}}{C_i + C_{gi} + C_{ti}} \quad (48)$$

with

$$q_0 = \frac{V_0}{2e} \sum_{i=R,L} C_{ti} \left(1 - \frac{C_{ti}}{C_i + C_{gi} + C_{ti}} \right). \quad (49)$$

The authors proposed to simplify equation (44) using a Born-Oppenheimer-like approximation. The transformer junction is assumed to be confined to its lowest energy band (so it acts like a variable capacitance). Then one can replace the "transformer" part of the Hamiltonian by the dispersion relation of its lowest band

$$-E_J \cos \phi + E_C [n - q(n_L, n_R)]^2 = \epsilon_0(q(n_L, n_R)) \quad (50)$$

This is similar to separating "fast" electronic and "slow" nuclei degrees of freedom in the original Born-Oppenheimer approximation. The approximation is valid when $E_J \gg E_{J_i}$ for $E_J \ll E_C$ and $\sqrt{E_C E_J} \gg E_{J_i}$ for $E_J \geq E_C$. In other words the characteristic energy gap between the bands of the transformer junction is much larger than the qubit energies. In the charge regime we identify the two states with zero and one excess Cooper pair on the island respectively as the qubit states described by Pauli matrices ($n_i = (\sigma_{zi} + 1)/2$). Then, assuming that the system in Fig. 16 is symmetric ($C_{g1}/(C_1 + C_{g1} + C_{t1}) = C_{g2}/(C_2 + C_{g2} + C_{t2}) = c$), one can express the dispersion relation of the lowest transformer junction band as follows :

$$\epsilon_0(q(n_L, n_R)) = \nu \sigma_{zL} \sigma_{zR} + \delta(\sigma_{zL} + \sigma_{zR}) + \mu \quad (51)$$

with

$$\nu = \frac{1}{4} (\epsilon_0(\tilde{q} + c) + \epsilon_0(\tilde{q} - c) - 2\epsilon_0(\tilde{q})) \quad (52)$$

$$\delta = \frac{1}{4} (\epsilon_0(\tilde{q} + c) - \epsilon_0(\tilde{q} - c)) \quad (53)$$

$$\mu = \epsilon_0(\tilde{q} + c) + \epsilon_0(\tilde{q} - c) + 2\epsilon_0(\tilde{q}) \quad (54)$$

$$\tilde{q} = q_0 + c \sum_i (q_i - 1/2) \quad (55)$$

The first term on the right-hand side in equation (51) describes the effective coupling between the qubits, the second term describes the shift of the qubit bias

and the third term is the constant. Equation (52) is the main result of [50]. The authors showed that the coupling constant ν can be positive and negative and thus is sign-tunable and therefore can be switched on and off. The coupling constant is controlled by the average induced charge \tilde{q} , which depends on the gate voltage V_0 .

3.3 Numerical results

Our goal now is to check to what extent the Born-Oppenheimer-like approximation is valid for E_{J_i} which are typical for real charge qubits and are of the order of a few % of E_{C_i} . For this we will compare the coupling coefficient ν described by equation (52) with the effective coupling coefficient calculated numerically. The qubits can be still considered in a charge qubit regime ($E_{J_i} \ll E_{C_i}$). This will simplify the calculations and for such system a convenient basis is formed by the charge states, parameterized by the number of Cooper pairs (n, n_R, n_L) on the islands. In this basis the Hamiltonian (44) reads

$$\begin{aligned}
H = & - \sum_{i=L,R} \frac{E_{J_i}}{2} (|0\rangle_i \langle 1|_i + |1\rangle_i \langle 0|_i) - \frac{E_J}{2} \sum_n (|n\rangle \langle n+1| + |n+1\rangle \langle n|) \\
& + \sum_{\substack{i=L,R \\ n_i=0,1}} E_{C_i} (n_i - q_i)^2 |n_i\rangle \langle n_i| + E_C \sum_{n, n_L, n_R} (n - q(n_L, n_R))^2 |n\rangle \langle n| |n_L\rangle \langle n_L| |n_R\rangle \langle n_R|. \quad (56)
\end{aligned}$$

We now calculate the eigenvalues of Eq. (56) by choosing the basis $|n_L n_R n\rangle$ and taking into account the levels of the transformer with the number of excess Cooper pairs from $-n$ to n . The matrix $\langle n n_R n_L | H | n_L n_R n \rangle$ has a block structure and consists of 16 (4×4) matrices ($N \times N$), where $N = 2n + 1$.

Here are the matrix elements:

- $\langle n 0 0 | H | 0 0 n' \rangle = (E_{CL} \cdot q_L^2 + E_{CR} \cdot q_R^2 + E_C \cdot (n - q(0, 0)))^2 \delta_{n, n'} - \frac{E_J}{2} (\delta_{n, n'+1} + \delta_{n+1, n'})$

- $\langle n00|H|01n'\rangle = -\frac{E_{JR}}{2}\delta_{n,n'}$
- $\langle n00|H|10n'\rangle = -\frac{E_{JL}}{2}\delta_{n,n'}$
- $\langle n00|H|11n'\rangle = 0$
- $\langle n10|H|00n'\rangle = -\frac{E_{JR}}{2}\delta_{n,n'}$
- $\langle n10|H|01n'\rangle = (E_{CL}\cdot q_L^2 + E_{CR}\cdot(1-q_R)^2 + E_C\cdot(n-q(0,1)))^2\delta_{n,n'} - \frac{E_J}{2}(\delta_{n,n'+1} + \delta_{n+1,n'})$
- $\langle n10|H|10n'\rangle = 0$
- $\langle n10|H|11n'\rangle = -\frac{E_{JL}}{2}\delta_{n,n'}$
- $\langle n01|H|00n'\rangle = -\frac{E_{JL}}{2}\delta_{n,n'}$
- $\langle n01|H|01n'\rangle = 0$
- $\langle n01|H|10n'\rangle = (E_{CL}\cdot(1-q_L)^2 + E_{CR}\cdot q_R^2 + E_C\cdot(n-q(1,0)))^2\delta_{n,n'} - \frac{E_J}{2}(\delta_{n,n'+1} + \delta_{n+1,n'})$
- $\langle n01|H|11n'\rangle = -\frac{E_{JR}}{2}\delta_{n,n'}$
- $\langle n11|H|00n'\rangle = 0$
- $\langle n11|H|01n'\rangle = -\frac{E_{JL}}{2}\delta_{n,n'}$
- $\langle n11|H|10n'\rangle = -\frac{E_{JR}}{2}\delta_{n,n'}$
- $\langle n11|H|11n'\rangle = (E_{CL}\cdot(1-q_L)^2 + E_{CR}\cdot(1-q_R)^2 + E_C\cdot(n-q(1,1)))^2\delta_{n,n'} - \frac{E_J}{2}(\delta_{n,n'+1} + \delta_{n+1,n'})$

By numerically diagonalizing this matrix we get the eigenvalues and eigenvectors and therefore the energy levels of our system.

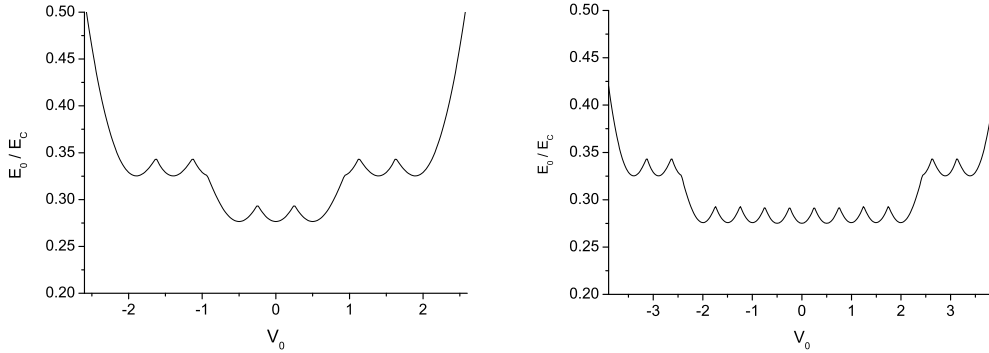


Figure 17: The lowest energy band of the system for $n = 1$ (left) and $n = 2$ (right).

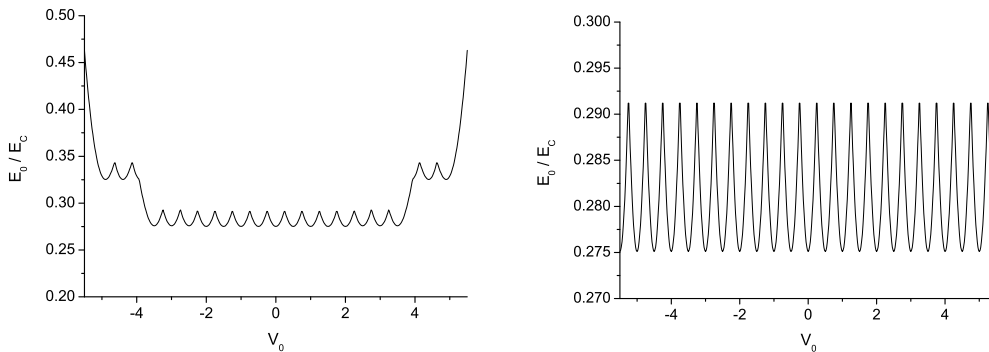


Figure 18: The lowest energy band of the system for $n = 3$ (left) $n = 10$ (right).

We will normalize all energies through the charging energy of the transformer junction and put the electron charge to $e = 1$. For the sake of simplicity we assume that the junction energy of the transformer is $\frac{1}{2}$ of its charging energy and the capacitance of all three Josephson junctions are the same.

We now have to choose the parameter n big enough, to calculate the lowest energy bands of the system as a function of the injected charge (gate voltage) with a high precision. Naturally, the wider the gate voltage range is that we are interested in, the more extra Cooper pairs on the transformer junction (n) we have to take into account. Figures 17 and 18 show the lowest energy band E_0 for different n .

To analyze the effective coupling between the qubits it is enough to consider \tilde{q} in the interval $[-0.5; 0.5]$. For our further calculations we put $n = 21$. Numerical

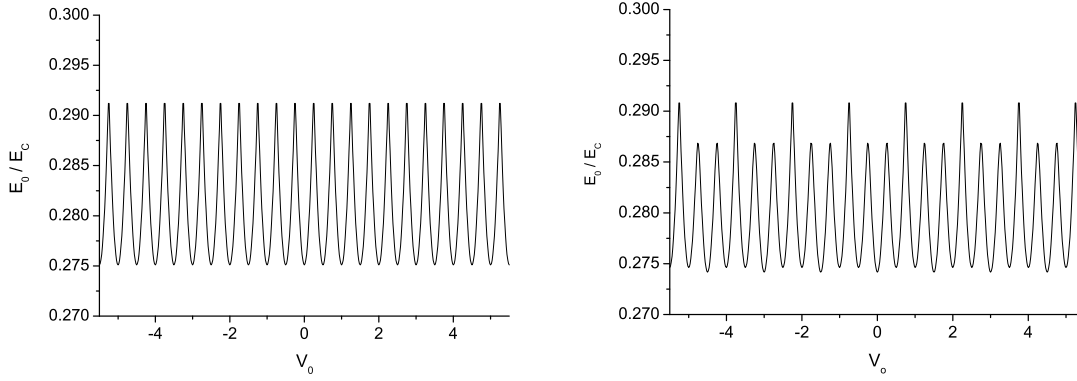


Figure 19: The lowest energy band of the system for $E_{Ji} = 0$ (left) and $E_{Ji} = 1\%E_{Ci}$ (right)

calculations show that this gives us the exact lowest energy levels of the system in the desired interval, while the matrix is still small enough (172×172) to be exactly diagonalized in a short time.

Now we are in the position to evaluate the lowest energy band of our system for different E_{Ji} , see Figs. 19-21. Here we put $c = 1/3$ in agreement with [50]. The results are logical. A non-zero value of E_{Ji} mixes the states of the qubits $\{\uparrow\downarrow\}$ and $\{\downarrow\uparrow\}$ (that are indistinguishable if our system is symmetric) with the states $\{\downarrow\downarrow\}$ and $\{\uparrow\uparrow\}$ due to the transitions. Here the state \downarrow represent the ground state and the state \uparrow the excited state of the charge qubit. The higher the Josephson energy of the qubit junction is, the bigger is the split between the energy bands and therefore the bigger is the influence on E_0 . There is also a small shift of the level to the zero point.

The value of the E_J - Josephson energy of the transformer - affects the influence of the E_{Ji} on the minimum energy level, see Figs. 22. As we can see, the mixing of the states is more effective with bigger E_J . The influence of the E_{Ji} on the lowest energy band of the transformer is similar to the influence on the minimum energy of the system, see Figs. 23, 24. We can see, that the energy of transformer increases with the increasing E_{Ji} , but the full energy - decreases. So the influence of the E_{Ji} on the qubits energy is more significant.

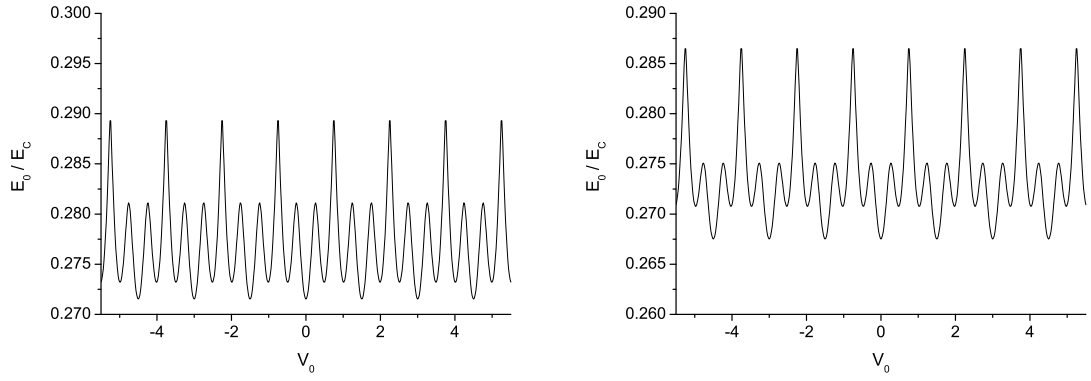


Figure 20: The lowest energy band of the system for $E_{Ji} = 2\% E_{Ci}$ (left) and $E_{Ji} = 3\% E_{Ci}$ (right)

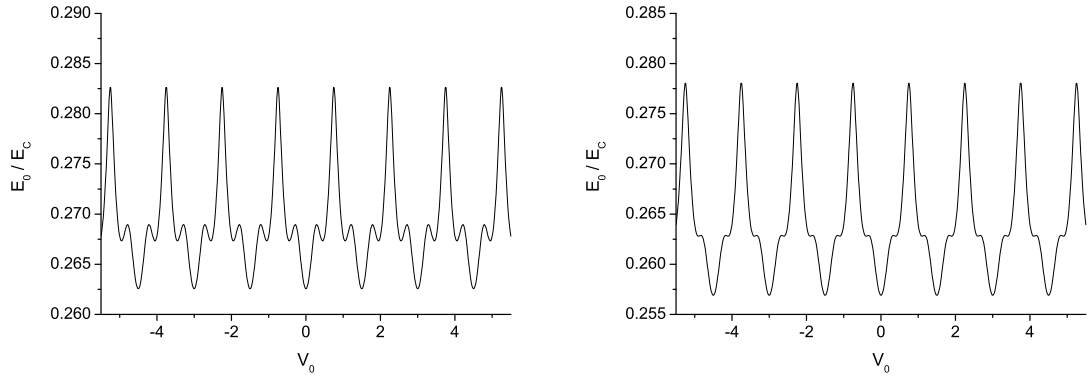


Figure 21: The lowest energy band of the system for $E_{Ji} = 4\% E_{Ci}$ (left) and $E_{Ji} = 5\% E_{Ci}$ (right)

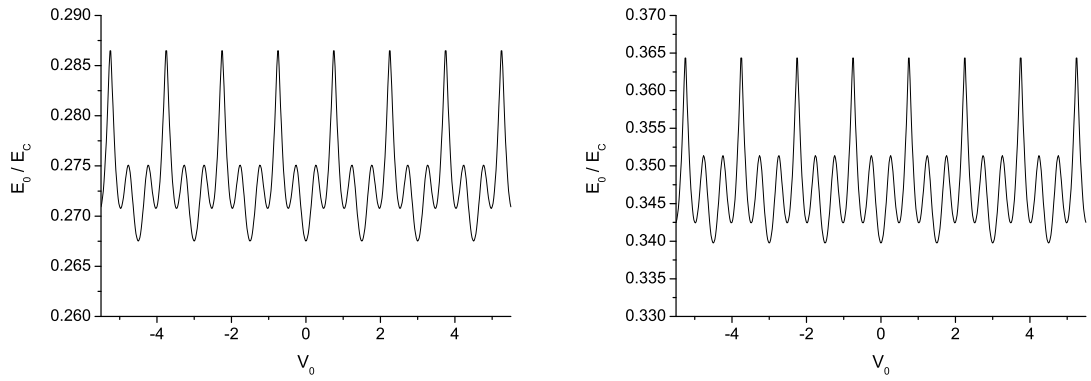


Figure 22: The lowest energy band of the system for $E_J = 0.5 E_C$ (left) and $E_J = 0.3 E_C$ (right), $E_{Ji} = 3\% E_{Ci}$

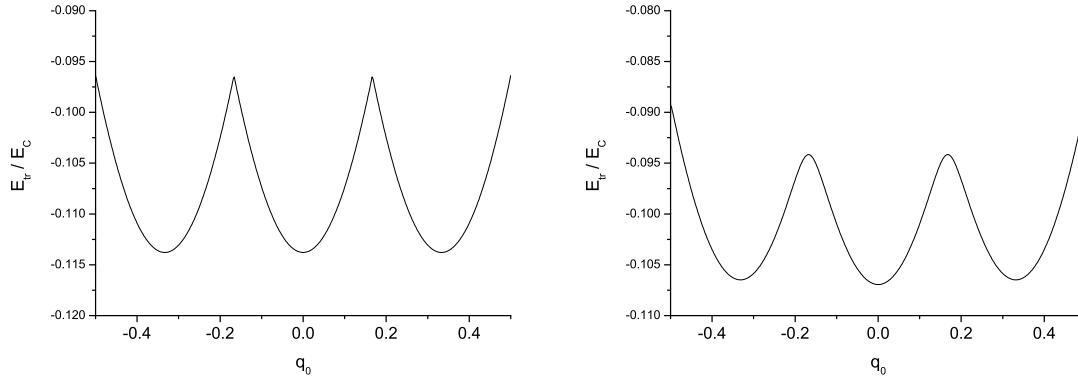


Figure 23: The lowest energy band of the transformer for $E_{Ji} = 0$ (left) and $E_{Ji} = 1\%E_{Ci}$ (right)

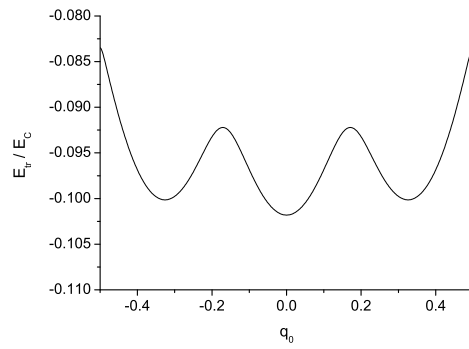


Figure 24: The lowest energy band of the transformer for $E_{Ji} = 2\%E_{Ci}$

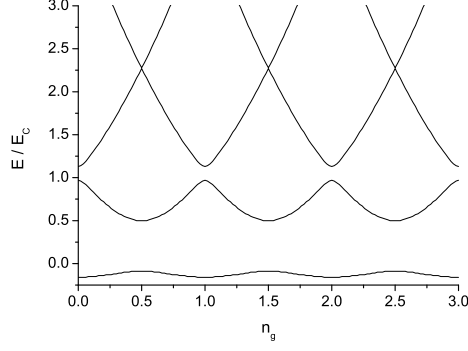


Figure 25: The lowest energy bands of the transformer junction.

Now we can check the validity of Born-Oppenheimer-like approximation. In the charge qubit regime the energy of the transformer is expressed as Eq. (51). We will write the formulas for ν , δ and μ once again:

$$\nu = \frac{1}{4} (\epsilon_0(\tilde{q} + c) + \epsilon_0(\tilde{q} - c) - 2\epsilon_0(\tilde{q}))$$

$$\delta = \frac{1}{4} (\epsilon_0(\tilde{q} + c) - \epsilon_0(\tilde{q} - c))$$

$$\mu = \epsilon_0(\tilde{q} + c) + \epsilon_0(\tilde{q} - c) + 2\epsilon_0(\tilde{q})$$

$$\tilde{q} = q_0 + c \sum_i (q_i - 1/2)$$

We will calculate the quantity ϵ_0 as a function of the injected charge using the same matrix method. It is well known function of the charge. The lowest energy bands of the transformer junction are shown in Fig. 25.

Figure 26 shows ν as a function of q_0 given by formula (51).

To check how ν depends on E_{Ji} we assume that Josephson energies of the qubit junctions, despite having non zero values, are small enough. Therefore the qubits are

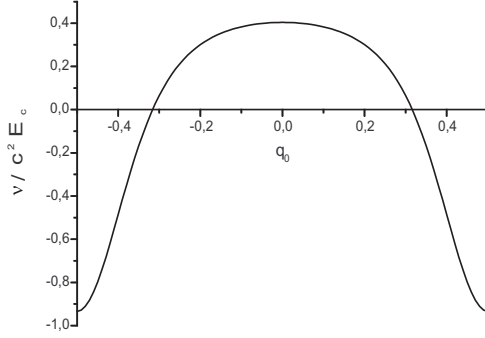


Figure 26: Coupling constant ν as a function injected charge q_0 for $c = 0.1$

still in the charge regime and formula (51) is valid with coefficients that now also depend on E_{Ji} . In this case the energies of different qubit states are

$$E_{\uparrow\uparrow} = 2\delta' + \nu' + E_{CL}(1 - q_L)^2 + E_{CR}(1 - q_R)^2, \quad (57)$$

$$E_{\uparrow\downarrow} = -\nu' + E_{CL}(1 - q_L)^2 - E_{CR}q_R^2, \quad (58)$$

$$E_{\downarrow\uparrow} = -\nu' - E_{CL}q_L^2 + E_{CR}(1 - q_R)^2, \quad (59)$$

$$E_{\downarrow\downarrow} = -2\delta' + \nu' - E_{CL}q_L^2 - E_{CR}q_R^2. \quad (60)$$

To simplify the analysis we put $E_{CL} = E_{CR}$ and $q_L = q_R = \frac{1}{2}$, so that $E_{\uparrow\downarrow} = E_{\downarrow\uparrow}$.

Knowing the lowest energy bands of our system and identifying them with Eqs. (57)-(60) we can calculate ν' and compare it with ν . However, one must remember, that in the regions, that are close to the points where the states are mixing we can not perform the identification and this method is not valid anymore. In this case one should use the whole Hamiltonian Eq. (44) with the transformer energy Eq. (51) and calculate ν' using its lowest energy bands. But as we are interested in relatively small value of $E_{Ji} \sim 1 - 4\%E_{Ci}$ (state mixing is small), we can use the formulas (57)-(60)

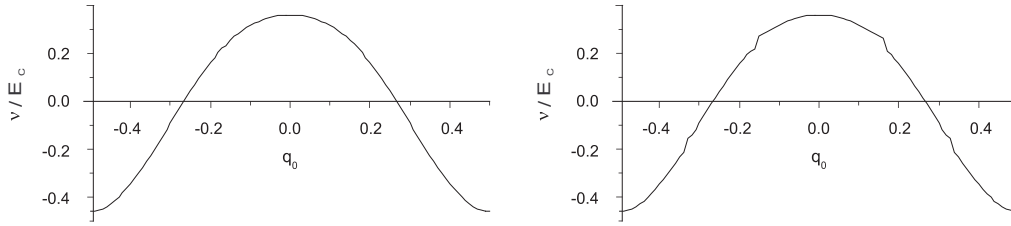


Figure 27: Coupling constant ν as a function injected charge q_0 for $E_{Ji} = 0$ (left) and $E_{Ji} = 1\%E_{Ci}$ (right).

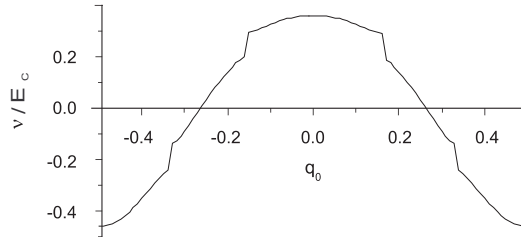


Figure 28: Coupling constant ν as a function injected charge q_0 for $E_{Ji} = 2\%E_{Ci}$.

almost for any value of gate voltage from the interval we are interested in. Results for $c = 0.3$ are show in Figs. 27, 28.

For better comparison with [50] we can draw the point from the "trusted" regions for $c = 0.1$ in one graph, see Fig. 29.

3.4 Conclusion

We can see that in the vicinity of the point where the coupling is switched off (which is the most important for realization of two qubit quantum gates) our simple method is valid and the influence of non zero values of E_{Ji} can be neglected. The coupling constant is changed slightly, but the point where ν is equal to zero is not affected by E_{Ji} . Therefore the Born-Oppenheimer-like approximation is valid for qubits in a realistic system if there are no other types of interactions between the qubits.

Recently, Hutter *et al* showed that the nonadiabatic, inductive contribution persists in this coupling scheme when the capacitive coupling is tuned to zero. On the other hand, the total coupling can be turned off (in the rotating wave approximation)

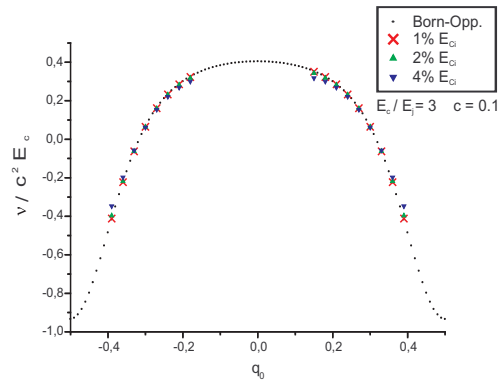


Figure 29: Coupling constant ν as a function injected charge q_0 for different E_{Ji} if the qubits are operated at the symmetry points.

4 Quantum state transfer in arrays of flux qubits

4.1 Introduction

As we have written in the introduction, the idea to use quantum spin chains for short-distance quantum communication was put forward by Bose [8]. The main results of Bose's work are independent of physical realizations of the spins and the spin-spin couplings. Quantum state transfer can be implemented using any type of two-level systems. However, it is preferable to use the technology that is adapted to the quantum information hardware that is supposed to be coupled by the transmission line. One of the most promising architectures of quantum computing devices are superconducting circuits, for example charge, flux and charge-flux qubits. In recent years these were intensively studied both theoretically and experimentally.

One possible realization of an effective transmission line for charge qubits was described in [61]. This was, to our knowledge, the first implementation of a solid-state quantum communication protocol following the idea of Bose. There, the fidelity of state transfer through Josephson junction arrays and the influence of static disorder and dynamical noise were analyzed. Authors also studied the readout process using single-electron transistor and its back action on the state transfer.

In this chapter we will consider a persistent-current qubit [36] and a line of such qubits [38] as a spin chain. We will show that it is appropriate for state transfer with high fidelity in systems containing flux qubits.

4.2 Persistent-current qubit arrays

A persistent current qubit is a superconducting loop with three Josephson junctions, see Fig. 30. First we will briefly describe the physics of this system following [37, 36]. We assume that the left and the right Josephson junctions have capacitance C and Josephson energy E_J , the central junction is characterized by a capacitance αC and

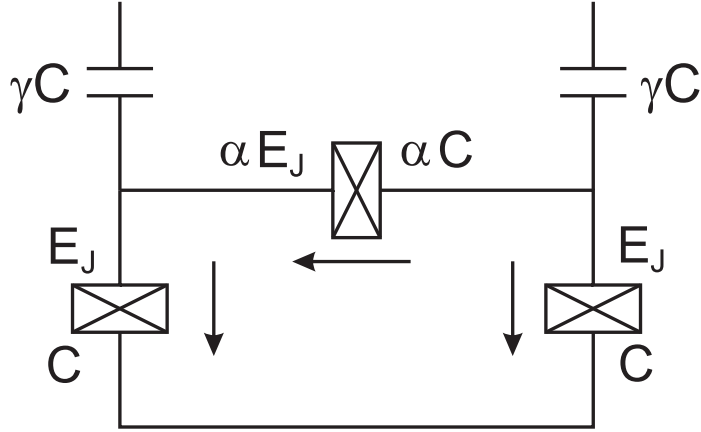


Figure 30: Persistent-current qubit [after [37]]

Josephson energy αE_J with $\alpha < 1$. The gate capacitances are equal to γC . Neglecting the inductance of the loop we can assume that the total flux through it is external flux Φ . Therefore flux quantization gives us $\phi_l + \phi_\alpha - \phi_r = -2\pi f$, where ϕ_l , ϕ_r and ϕ_α are the gauge-invariant phases of the left, right and central junctions respectively and f is the magnetic frustration, i.e. the amount of external magnetic flux in the loop in units of the flux quantum $\Phi_0 = h/(2e)$. We also assume the same direction of the currents as in [37]. Now we are in the position to write the Josephson energy of the system as

$$\frac{U_J(\phi_l, \phi_r)}{E_J} = 2 + \alpha - \cos \phi_l - \cos \phi_r - \alpha \cos(2\pi f + \phi_l - \phi_r) \quad (61)$$

for a certain range of magnetic frustration f , U_J as a function of phases ϕ_l and ϕ_r has two stable configurations. They correspond to the clockwise and counterclockwise currents in the loop and repeat in a phase space, since (61) is 2π -periodic function of its arguments, see Fig. 31. We will neglect the tunneling between different cells with two minima [36] and will consider the qubit dynamics only within one cell, see Fig. 32. In this case our system can be approximated as a two level system with Hamiltonian

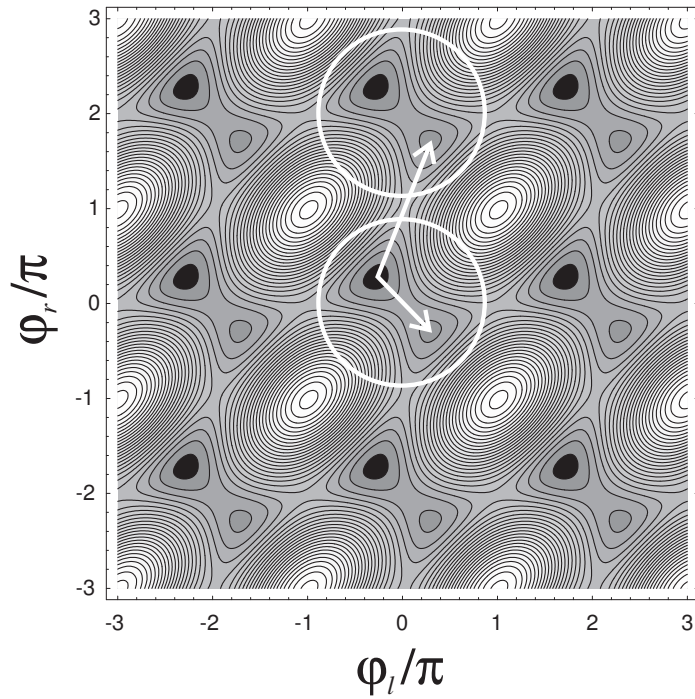


Figure 31: Josephson energy of qubit as a function of phases for $\alpha = 0.8$ and $f = 0.48$. Circles mark cells with two minima. The arrows indicate tunneling within one cell and between two cells.

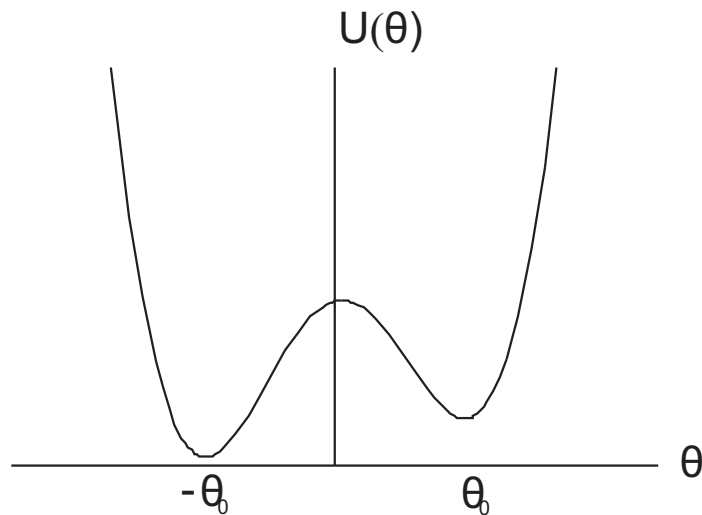


Figure 32: Josephson energy as a function of the phase difference $\theta = \phi_l - \phi_r$ along the shorter arrow in Fig. 31

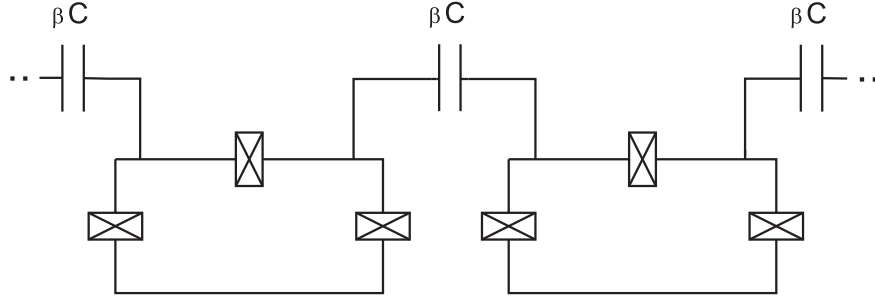


Figure 33: Capacitively coupled qubits.

$$H_0 = -\Delta_0 \sigma^x - B \sigma^z \quad (62)$$

that is the same as that of a spin- $\frac{1}{2}$ particle in a magnetic field. The eigenstates $|0\rangle \equiv |\downarrow\rangle$ and $|1\rangle \equiv |\uparrow\rangle$ of σ^z correspond to clockwise and counterclockwise currents (minima within one cell in Fig. 31). The coefficient Δ_0 is a tunneling amplitude between these states and its exact expression as a function of the system parameters will be given later. The effective magnetic field B is determined by the modulus of the circulating current I_p and the external magnetic flux Φ

$$B = I_p(\Phi) \left(\Phi - \frac{1}{2} \Phi_0 \right), \quad (63)$$

The circulating current I_p depends on the magnetic frustration.

We assume, that the temperature is low enough, i.e. $k_B T$ is smaller than the energy of the state $|1\rangle$, so we can neglect thermal fluctuations.

Persistent-current qubits can be capacitively coupled (with coupling capacitance βC , see Fig. 33) to form a one-dimensional array [38], that for $\beta \gg 1$ has the Hamiltonian

$$H = - \sum_{i=2}^N [J_{xy}(\sigma_i^+ \sigma_{i-1}^- + \sigma_i^- \sigma_{i-1}^+) + J_z \sigma_i^z \sigma_{i-1}^z] - \sum_{i=1}^N (\Delta \sigma_i^x + B \sigma_i^z). \quad (64)$$

The terms $J_z \sigma_i^z \sigma_{i+1}^z$ are due to the small inductive coupling between adjacent

qubits. Here $J_z = 2M_{q,q}I_p^2$, where $M_{q,q}$ is their mutual magnetic inductance. The coupling constant J_z could in principle be increased by a common Josephson junction between two neighboring qubits [38]. However calculations show that smaller J_z is preferable for good state transfer and therefore we will consider only weak coupling without any amplification. The Hamiltonian (64) contains the term $\Delta \sum_i \sigma_i^x$, i.e. it does not conserve the z-component of the total spin (which is equivalent to the number of sites in the excited state $|1\rangle$). Therefore, the theory proposed in [8] is not valid in our case. However, if $\beta \gg 1$ Δ is much less than J_{xy} [38] and we can neglect this term at first. Later we will use perturbation theory to analyze how nonzero values of Δ affect the results.

The tunneling amplitude Δ between the states $|0\rangle$ and $|1\rangle$ of the coupled qubits differs from the value Δ_0 for individual non-coupled qubits. As we will see later, this is due to the fact that coupling suppresses independent tunneling events in which only one qubit changes its state. Also, simultaneous tunneling events $|11\rangle \longleftrightarrow |00\rangle$ for two neighboring qubits are suppressed and therefore we neglect such processes in our model. Correlated tunneling events $|10\rangle \longleftrightarrow |01\rangle$ are unaffected by the coupling.

We assume that the gate capacitances are equal to γC and use quasiclassical approach described in [37] to calculate Δ and J_{xy} . The idea is to represent the dynamics of the qubit by motion of a fictitious particle in the potential (61), see also Fig. 32. Under this approximation, Δ_0 can be obtained by the WKB method as

$$\Delta_0 = \sqrt{E_J E_C} \sqrt{\frac{2(4\alpha^2 - 1)}{\alpha(1 + \gamma)}} \exp\left(-\frac{4}{\hbar} \sqrt{M\alpha E_J} \left(\sqrt{1 - \alpha^2/4} - \frac{\arccos(\alpha/2)}{2\alpha}\right)\right) \quad (65)$$

where

$$M = \frac{\hbar^2}{E_C} \frac{1 + 2\alpha + \gamma}{4}. \quad (66)$$

is effective mass of the fictitious particle.

We now want to consider two interacting qubits that are coupled by a capacitor βC , see Fig. 33. The collective dynamics of the two qubits can be described by the motion of a fictitious particle in a two-dimensional potential (parameterized by qubit phase differences θ_1 and θ_2) with four minima. The kinetic energy is the associated Coulomb charging energy of the junction capacitances, while the potential energy corresponds to the Josephson energy of the qubits and is equal to the sum of the Josephson contributions of both qubits. When two qubits are connected by the capacitor, kinetic energy gets the extra term [38]

$$T_{coupl} = \frac{m^*}{8}(\dot{\theta}_1 + \dot{\theta}_2)^2, \quad (67)$$

where

$$m^* = (\hbar/2e)^2 \beta C. \quad (68)$$

In this case the effective mass to move in $(0,0) \leftrightarrow (1,1)$ direction (see Fig. 34) is $M + 2m^*$, the effective mass for independent qubit tunneling events is $M + m^*$ and the effective mass for tunneling in $(1,0) \leftrightarrow (0,1)$ direction is equal to M . From these formulas one can see that the tunneling is suppressed in all directions except $(1,0) \leftrightarrow (0,1)$, if $m^* \gg M$. Due to this fact state transfer with high fidelity is possible.

We will also use the WKB-method to obtain Δ and J_{xy} . Namely we will describe the tunneling amplitude through some potential barrier $U(x)$, see Fig. 35, for a particle with effective mass m and energy E as

$$t = \frac{\hbar\omega}{2\pi} \exp \left[-\frac{i}{\hbar} \int_{x_1}^{x_2} \sqrt{2m(E - U(x))} dx \right] \quad (69)$$

where ω is the attempt frequency to escape the potential well. To calculate Δ

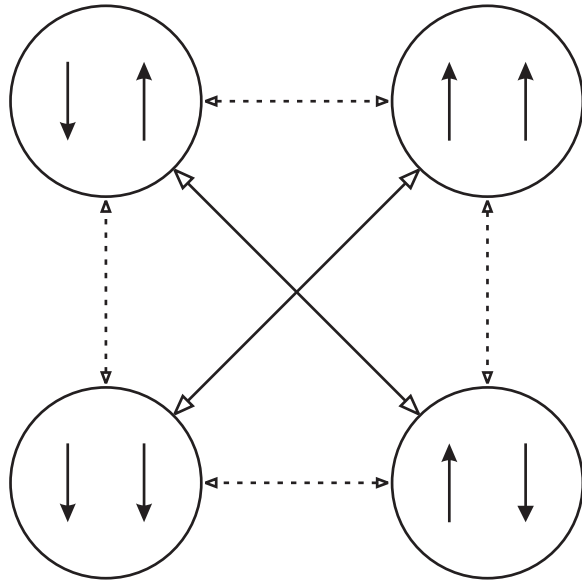


Figure 34: Tunneling in capacitively coupled qubits.

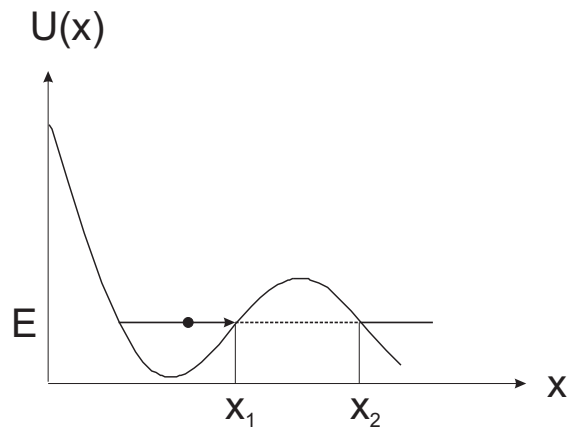


Figure 35: Particle with energy E escaping the potential well described by $U(x)$.

we simply use formula (65) taking into account the new effective mass $M + m^*$ and therefore multiplying the expression in the exponent by

$$\sqrt{\frac{M + m^*}{M}} = \sqrt{1 + \frac{\beta}{2(1 + 2\alpha + \gamma)}} \quad (70)$$

To calculate J_{xy} we have to take into account, that the tunneling rate in $(1, 0) \leftrightarrow (0, 1)$ direction (WKB-calculation gives extra factor 2 in the exponent in (65)) is contributed by two terms of our Hamiltonian. One part of it is described by Δ -term and correspond to independent qubit tunneling. It is proportional to $(\frac{\Delta}{\hbar\omega})^2$. Second part is described by J_{xy} -term and corresponds to correlated tunneling of two cubits. It is equal to $4J_{xy}$ since

$$\langle 10 | J_{xy} (\sigma_1^+ \sigma_2^- + \sigma_1^- \sigma_2^+) | 01 \rangle = 4J_{xy} \quad (71)$$

To simplify the form of the expressions for Δ and J_{xy} we will use realistic qubit parameters from [37] and [36], namely $\alpha = 0.75$, $\gamma = 0.02$

$$\Delta = \Delta_0 \exp(-0.49 \sqrt{E_J/E_C} (\sqrt{1 + \beta/5} - 1)) , \quad (72)$$

$$4J_{xy} = \Delta_0 e^{-0.49 \sqrt{E_J/E_C}} \left(1 - e^{-0.98 \sqrt{E_J/E_C} (\sqrt{1 + \beta/5} - 1)} \right) . \quad (73)$$

With $E_J/E_C \approx 100$, we obtain

$$\Delta/\Delta_0 = \exp(-4.9(\sqrt{1 + \beta/5} - 1)) . \quad (74)$$

Therefore, independent tunneling is effectively suppressed for $\beta \sim 10$. Δ and $4J_{xy}$ coincide for $\beta = 15$. For $\beta = 20$, $4J_{xy}$ is three times larger and for $\beta = 30$ it is 25 times larger than Δ . In this case, as we will show later, Δ can be neglected for short chains.

For $\Delta = 0$, the Hamiltonian (64) is that of an asymmetric (XXZ) Heisenberg model in the presence of a magnetic field,

$$H_L = - \sum_{i=2}^N [J_{xy}(\sigma_i^+ \sigma_{i-1}^- + \sigma_i^- \sigma_{i-1}^+) + J_z \sigma_i^z \sigma_{i-1}^z] - \sum_{i=1}^N B \sigma_i^z. \quad (75)$$

We now want to calculate the fidelity of the state transfer. The chain is initialized in the state $|00\dots 00\rangle$ by first choosing a large negative value for the parameter B , see Eqs. (75) and (63). Then, the first qubit is prepared in the state $|\psi_{in}\rangle$ i.e., the total state of the array is $|\psi_{in}, 00\dots 00\rangle$. This is not an eigenstate of the Hamiltonian (75), therefore the system will evolve in time. After some time t the state of the last qubit is read out. In general the last qubit will be in a mixed state, which is described by a density matrix ρ_{out} . As wrote earlier in introduction, we average the fidelity over all pure input states on the Bloch sphere

$$F(t) = \frac{1}{4\pi} \int \langle \psi_{in} | \rho_{out}(t) | \psi_{in} \rangle d\Omega \quad (76)$$

to obtain a quantity $1/2 \leq F(t) \leq 1$ that measures the quality of transmission independent of $|\psi_{in}\rangle$.

4.3 Fidelity of the state transfer

As written in the introduction, we perform our calculations in the basis $|k\rangle = |00\dots 010\dots 0\rangle$ for which the spin in the k -th qubit is in the state $|1\rangle$ and all others are in the state $|0\rangle$. The Hamiltonian (75) of the array commutes with the z-component of the total spin $\sum_i \sigma_i^z$. Therefore we can use the results of [8] to calculate the average fidelity in terms of $f_{1,N}(t) = \langle 1 | e^{-iH_L t} | N \rangle$ i.e., the transition amplitude of the excitation over the array. The average fidelity can then be expressed as

$$F(t) = \frac{1}{2} + \frac{|f_{1,N}(t)|^2}{6} + \frac{|f_{1,N}(t)| \cos(\gamma)}{3}, \quad (77)$$

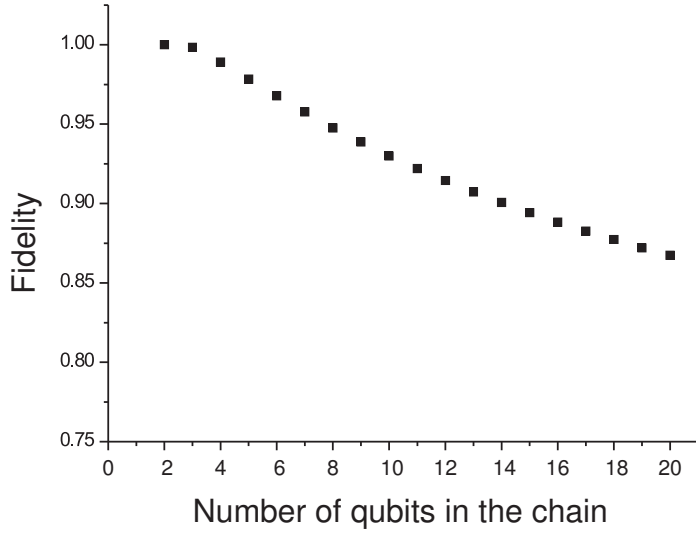


Figure 36: The first fidelity maximum for an array with $\alpha = 0.75$, $\gamma = 0.02$, $E_J/E_C = 100$, $\beta = 30$ and $E_J = 3\text{GHz}$, $a = 0.1$.

where $\gamma = \text{Arg}(f_{1,N}(t))$ is the argument of the complex quantity $f_{1,N}(t)$.

Varying the magnetic field one can make γ a multiple of 2π to maximize the average fidelity, such that the maximum fidelity will correspond to the maximum of $|f_{1,N}(t)|$. From here on we will assume that this is the case and therefore put $f_{1N} = |f_{1N}|$ when plotting fidelities of the state transfer. Furthermore, the fidelity of any state transfer is unity, if the modulus of the amplitude to transmit the state $|1\rangle$ across the array is unity.

We will now calculate $|f_{1,N}^N(t)|$ in the case $\Delta = 0$. The eigenfunctions of H_L can be described as follows:

$$|\tilde{k}\rangle = \sum_{n=1}^N b_{k,n}|n\rangle. \quad (78)$$

From the Schrödinger equation

$$H_L|\tilde{k}\rangle = (B(N-2) - J_z(N-5))|\tilde{k}\rangle - 2J_z(b_{k,1}|1\rangle + b_{k,N}|N\rangle) - 4J_{xy}(b_{k,2}|1\rangle + \sum_{n=2}^{N-1} (b_{k,n-1} + b_{k,n+1})|n\rangle + b_{k,N-1}|N\rangle), \quad (79)$$

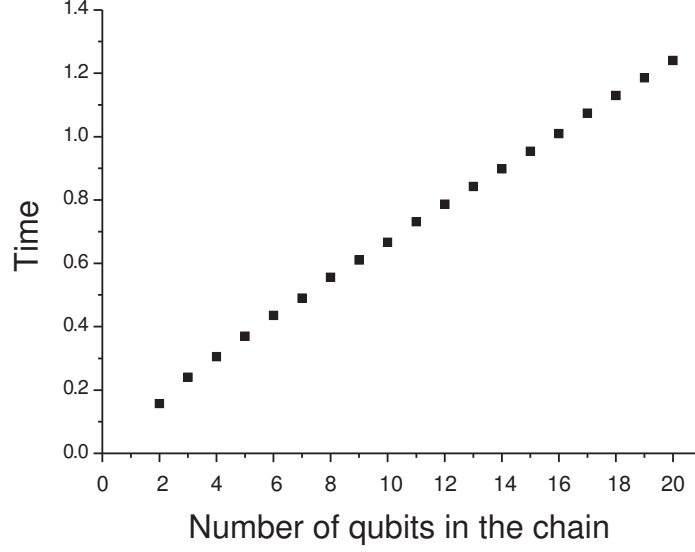


Figure 37: Time (in units of $1/E_J$) at which the first fidelity maximum is achieved. It is proportional to the length of the chain and depends on the coefficient J_{xy} .

we obtain the following system of equations for the coefficients $b_{k,n}$

$$\begin{cases} b_{k,n-1} + b_{k,n+1} = Db_{k,n} & (n \in [2, N-1]) \\ ab_{k,1} + b_{k,2} = Db_{k,1} \\ ab_{k,N} + b_{k,N-1} = Db_{k,N} \end{cases} \quad (80)$$

where $a = J_z/2J_{xy}$ and D is a constant. From the first two equations $b_{k,i}$ can be expressed in terms of $b_{k,1}$ as

$$b_{k,i} = P_i(D_k)b_{k,1}, \quad (81)$$

here $D_k, k = 1, \dots, N$ are the roots of

$$(D - a)P_N(D) = P_{N-1}(D). \quad (82)$$

$P_i(D)$ is a polynomial, that is determined recursively

$$P_1 = 1, \quad P_2 = D - a, \quad P_i = DP_{i-1} - P_{i-2}, \quad i = 3, \dots, N. \quad (83)$$

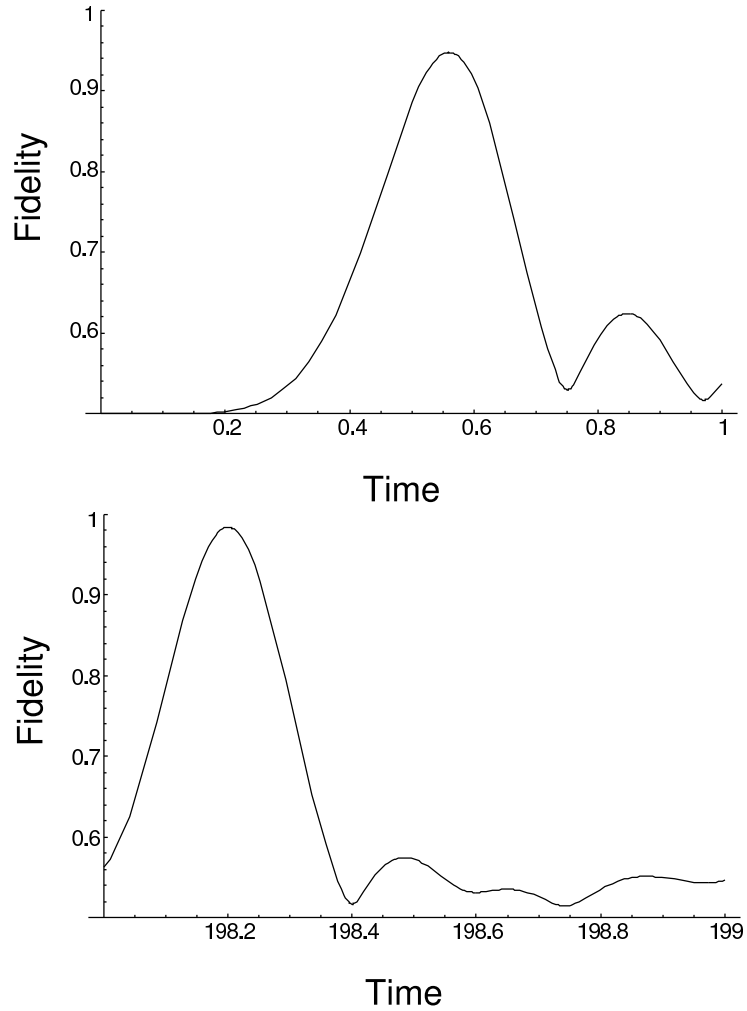


Figure 38: Fidelity as a function of time (in units of $1/E_J$) for a chain with $N = 8$. Upper panel: first fidelity maximum at small times. Lower panel: fidelity maxima around $t = 198$. The parameters are chosen as in Fig. 36.

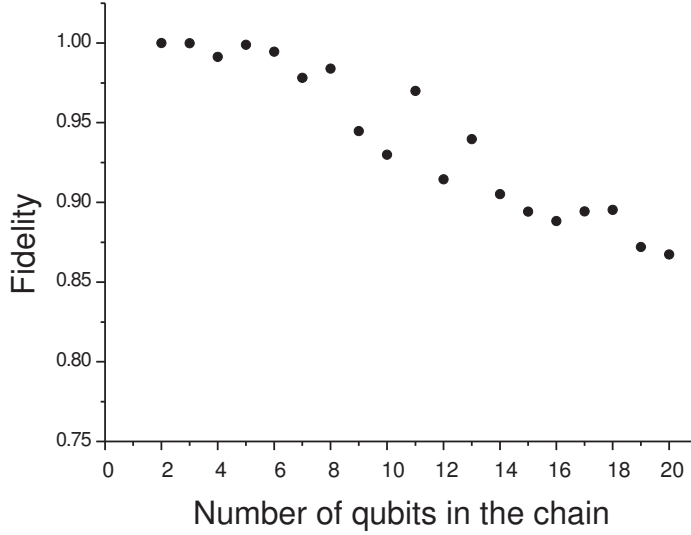


Figure 39: Fidelity maxima for times less than $4000/J_z$, all the chain parameters are as in Fig. 36.

The coefficient $b_{k,1}$ can be found from the normalization conditions

$$\langle \tilde{k} | \tilde{m} \rangle = \delta_{k,m} \Rightarrow b_{k,1}^2 = \frac{1}{P_1^2(D_k) + \dots + P_N^2(D_k)}. \quad (84)$$

Thus we have determined the eigenfunctions of the Hamiltonian and can find its eigenenergies

$$E_k = -J_z(N-5) + B(N-2) - 4D_k J_{xy}. \quad (85)$$

Setting $E_0 = 0$, we obtain

$$E_k = 2B + 4J_z - 4D_k J_{xy}. \quad (86)$$

The transition amplitude of the excitation through the array is given by

$$f_{1,N}(t) = \sum_{k=1}^N \langle \tilde{k} | 1 \rangle \langle N | \tilde{k} \rangle e^{-iE_k t} = \sum_{k=1}^N b_{k,1} b_{k,N} e^{-iE_k t}. \quad (87)$$

Using these formulas we have numerically calculated the average fidelities for different chain lengths and ratios $a = J_z/2J_{xy}$. The most relevant quantities for

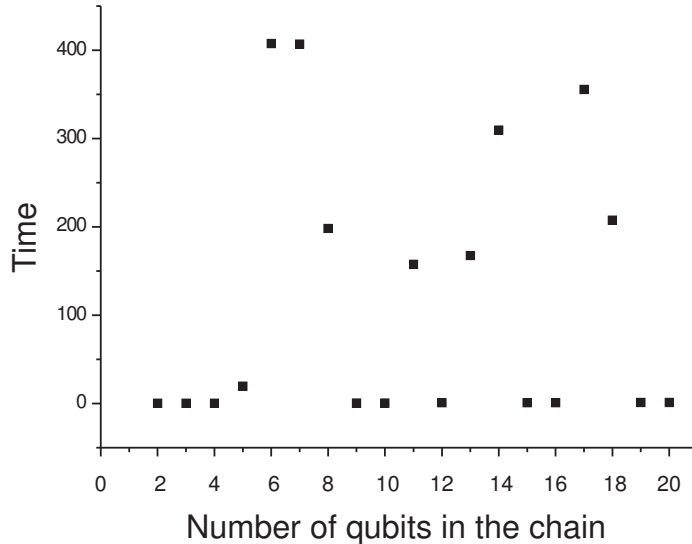


Figure 40: Times (in units of $1/E_J$) at which the fidelity maxima in Fig. 39 are achieved.

practical purposes are the first fidelity maxima, see Fig. 36 and Fig. 37, that we will call “fidelity” in the rest of this chapter.

For short-length chains the average fidelity is higher than 0.9. This makes persistent qubit arrays good candidates for transmission lines in quantum computers, that are based on flux degrees of freedom. Also they can be effectively used in the two-chain method proposed for achieving perfect state transfer [20]. The fidelity has a complicated oscillating behavior as a function of time, see Fig. 38. There are many local maxima, and the first of them is usually not the global maximum. Therefore, waiting long enough, we can achieve a higher fidelity. This can be seen by comparing Fig. 36 and Fig. 39.

However, the waiting times, i.e. the times, at which the maximum peaks of the fidelity shown in Fig. 39 occur are much longer than for the first maximum, see Fig. 40. Therefore, from the practical point of view the first maxima in the fidelity are more relevant.

Decoherence is another important reason why practical realizations of our proposal would have to focus on the first fidelity maximum. Like any physical realization of

a qubit, flux qubits are characterized by a finite dephasing time, and in a recent experiment times of order $\tau_\phi \approx 20\text{ns}$ were reported for a *single* flux qubit [33]. The time for the appearance of the first fidelity maximum is of order $\hbar L/E_J$. Therefore as a simple estimate of the effects of decoherence, we compare this time with the dephasing time, which leads to a limit of the length of the array of $L \sim \tau_\phi E_J/\hbar \sim 100$. Additional maxima after the first one will be further reduced by decoherence since they correspond to states traversing the array more than once.

To maximize the fidelity $\gamma = \text{Arg}(f_{1,N}(t))$ has to be chosen equal to zero. This can be done by varying the magnetic field, so that $-2Bt + \gamma_0 = 2\pi n$. Here γ_0 is transition amplitude phase for $B = 0$. To achieve more control of the qubit parameters the central junction can be replaced by a SQUID [37].

The works of Bose [8] and Christandl *et al.* [12] correspond to spin chains with a particular form of the Hamiltonian H_L ($J_z/2J_{xy} = 1$, $J_z/2J_{xy} = 0$). We have checked that in these limits our results agree with [8] and [12].

As mentioned above, the Hamiltonian of the real chain contains the term $\Delta \sum_{i=1}^N \sigma_i^x$, that does not conserve the z-component of the total spin (i.e. the number of excitations). Δ is small, however, i.e. we can use perturbation theory to analyze the influence of this term on the average fidelity. In this case we need to do calculations in a larger $(2^N + 1)$ -dimensional space, because in principle any number of excitations is possible. One can easily show, that in zero-order approximation the fidelity and the $N + 1$ lowest eigenstates will be the same as in the unperturbed case. The first-order corrections are zero, because $\langle k | \sigma_i^x | k \rangle = 0$ for the lowest eigenstates. So only the second-order terms, which are proportional to Δ^2 , affect the fidelity. The influence of the symmetry-breaking term therefore vanishes quadratically with Δ .

From Fig. 41 one can see that for qubits with the parameters mentioned in Fig. 36 it is sufficient to choose coupling capacitors with about 25-30 times the junction capacitance. In this case we can neglect the influence of Δ . For long times this

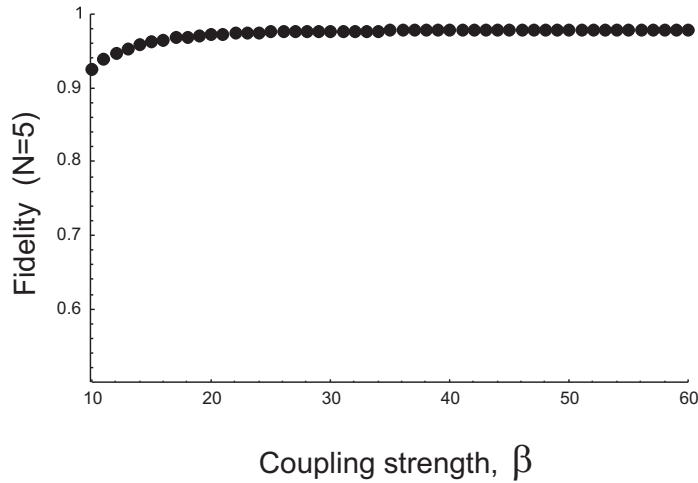


Figure 41: Fidelity dependence on β for chain length $N = 5$.

term becomes more important. This is another reason why only the first maxima are useful for practical realizations of high-fidelity transmission lines. One can, in principle, raise β to make the Δ -term less important for the maxima that occur later, but in this case the charging energy will increase and this will influence the fidelity and the properties of the qubit.

Conclusion

We have shown that a persistent-current qubit array is a good candidate for quantum state transfer with high fidelity in flux-qubit based quantum computers. For short-length chains the average fidelity of state transfer is higher than 0.9. Therefore, this type of array can be effectively used in the two-chain algorithm [20] for achieving perfect state transfer. The influence of the term proportional to $\Delta\sigma^x$, that does not commute with the z-component of the total spin, is quadratic in Δ and can be neglected at small times for $\beta \gg 1$.

5 Use of dynamical coupling for improved quantum state transfer

5.1 Introduction

We have seen above that efficient short-distance quantum state transfer is an important problem in the field of quantum computing. If we neglect relaxation and decoherence processes, then practical realization of the efficient quantum state transfer will have two problems to be solved. First is an efficient protocol, that provides high fidelity. As we wrote in introduction, a number of protocols of different nature were proposed in the last five years to improve the quality of the state transfer in spin chains. In all of them we have to use additional resources to raise the fidelity, that is quite natural trade-off for information sciences. It can be extra time needed for state transfer in the "weak coupling" proposals [24, 25], extra chain or chains for dual- and multi-rail encoding [20, 23], extra qubits to be controlled for encoding the information in Gaussian-like wave packets [22] or time-dependent coupling between the first and last pairs of qubits [27]. Only engineered couplings allow us to improve fidelity without extra resources used, but in this case F is more sensitive to disorder in qubit/coupling parameters.

While concentrating on improving the fidelity of the state transfer *per se* many papers ignored another fact that limits practical use of spin chains as transmission lines: the time interval for which the fidelity is high is very small for physical qubits and realistic qubit coupling parameters. For example, for the chain of flux qubits [62] with realistic experimental parameters [37], the half-width of the first fidelity maximum is about 0.2ns. At these time scales state readout and manipulation is impossible using current experimental technology. In this chapter we show that by dynamically varying the coupling constants only between the first and last pair of qubits we can solve this problem and also increase the fidelity of the state transfer.

In real chains the state to be transmitted is initialized in the first qubit, and this process must not influence the fidelity and dynamics of the chain. The most natural idea for a full transferring protocol is as following: to initialize the state in the first qubit, that is decoupled from the rest of the chain, then adiabatically couple it, wait a certain time and then adiabatically decouple the last qubit from the chain [63]. This method requires two controllable gates like one of the proposals for achieving perfect state transfer [27]. However in this chapter, the main purpose of the gates is to localize the state on the last qubit where it can be manipulated during times that are comparable to the decoherence/relaxation times.

5.2 Time-dependent coupling constants

As in the previous chapters we consider the XXZ-Hamiltonian as a model Hamiltonian. The XX-part of the Hamiltonian describes the tunneling of the excitation from one site to another and is a necessary requirement for quantum state transfer. Here, however, we will use time-dependent coupling constants between the first and last pair of qubits:

$$\begin{aligned}
H(t) = & -J_{xy1}(t)(\sigma_2^+ \sigma_1^- + \sigma_2^- \sigma_1^+) - J_{xy} \sum_{i=3}^{N-1} (\sigma_i^+ \sigma_{i-1}^- + \sigma_i^- \sigma_{i-1}^+) \\
& - J_{xyN}(t)(\sigma_N^+ \sigma_{N-1}^- + \sigma_N^- \sigma_{N-1}^+) - J_z \sum_{i=2}^N \sigma_i^z \sigma_{i-1}^z - B \sum_{i=1}^N \sigma_i^z. \quad (88)
\end{aligned}$$

The time-dependent coupling constants can be realized by varying the gate voltages on the 1st/2nd and $(N-1)$ th/ N th qubits for the flux qubit chain, or by replacing the Josephson junction between the charge qubits with a SQUID and varying the flux through it. One can also use a transformer scheme described in Chapter 3 as a variable capacitance between the flux qubits.

As a model we use “Fermi-function like” coupling constants:

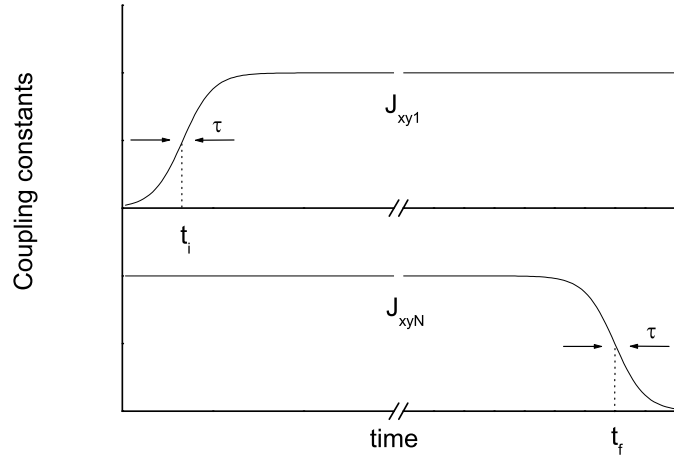


Figure 42: Coupling constants J_{xy1} and J_{xyN} as functions of time and coupling parameters.

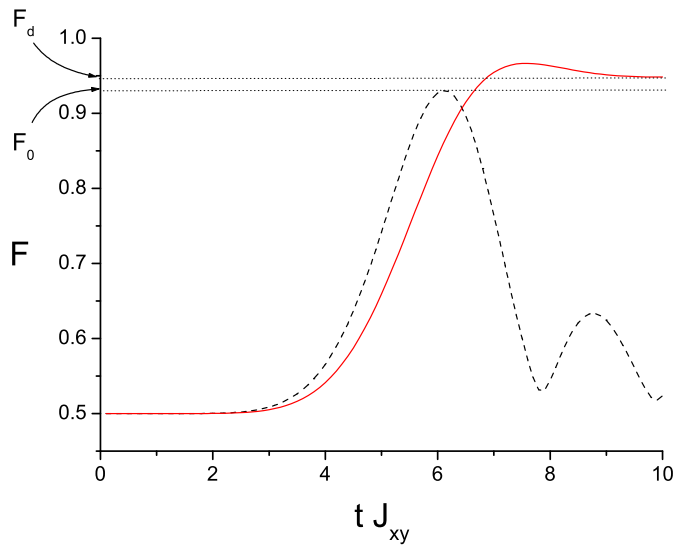


Figure 43: Fidelity as a function of time (in units of J_{xy}^{-1}) for a chain with constant coupling parameters (dashed line) and time-dependent coupling parameters (solid line), $N = 10$, $t_i = 0$, $t_f = 6.2/J_{xy}$, $\tau = 1/J_{xy}$.

$$\begin{aligned}
J_{xy1}(t) &= J_{xy}f(t_i, t) \\
J_{xyN}(t) &= J_{xy}f(t, t_f),
\end{aligned}
\tag{89}$$

with

$$f(t, t') = \frac{1}{1 + \exp \frac{t-t'}{\tau}}.
\tag{90}$$

These are smooth functions that vary from 0 (no coupling) to J_{xy} (full coupling) and vice versa, see Fig. 42. The time scale of the coupling/decoupling procedure is determined by τ . Instant coupling/decoupling corresponds to $\tau = 0$. Later we will use another type of coupling/decoupling functions to show that main results of this chapter are independent of our choice (89). The main reason why we use it first is simplicity of varying the coupling parameters.

As earlier in this thesis we will characterize the quality of the state transfer by fidelity. As usual, we assume that the chain is initialized in the state $|00\dots 00\rangle$. Then, the first qubit is prepared in the state $|\psi_{in}\rangle$, i.e. the total state of the array is $|\psi_{in}, 00\dots 00\rangle$. However if earlier after a time t the state of the last qubit was simply read out instantly, now we will analyze the fidelity after some longer time $t_d > t_f$, when the last qubit can be considered as completely decoupled from the rest of the chain.

By numerically solving the Schrödinger equation for the time-dependent Hamiltonian (88) we get the fidelity of the state transfer as a function of time and the coupling parameters τ , t_i and t_f . The fidelity has a complex oscillating behavior. Our goal is to find the coupling parameters that allow us to localize the state at the last qubit by decoupling it from the rest of the chain so that the fidelity is maximal. In comparing this fidelity with the static case, we concentrate on the first maximum: higher maxima appear only after times much longer than the time at which the first one occurs [62, 61]. The typical behavior of $F(t)$ for the static chain in the vicinity

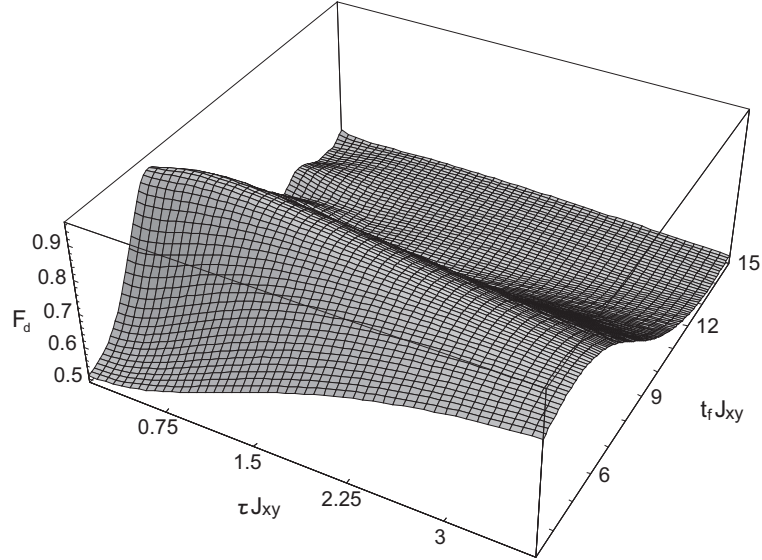


Figure 44: Stationary value of the fidelity after decoupling as a function of τ and t_f , $N = 10$, $t_i = 0$.

of the first maximum is shown in Fig. 43 (dashed line).

Figure 43 also shows the fidelity in the presence of time-dependent coupling constants (solid line). One can clearly see that at large times the state is localized at the last qubit with a fidelity F_d that is higher than for static coupling constants. The time at which the maximum is achieved is slightly larger. This is natural since in the presence of the coupling/decoupling procedure the transmission of the information from the first qubit to the chain and then to the last qubit is slower. After decoupling, the localized state can be manipulated during the time interval comparable with the decoherence and relaxation times for the qubit, which are several orders of magnitude longer than the half-width of the first fidelity maximum in the static case in present experimental setups. We would like to mention that the first fidelity maximum in the case of dynamical coupling constants is even higher than the stationary value of the fidelity after decoupling. Numerical calculations show that it can exceed the value 0.99, i.e. above threshold needed for quantum error correction. However, in this case, after the full decoupling the fidelity will go down to about 0.9.

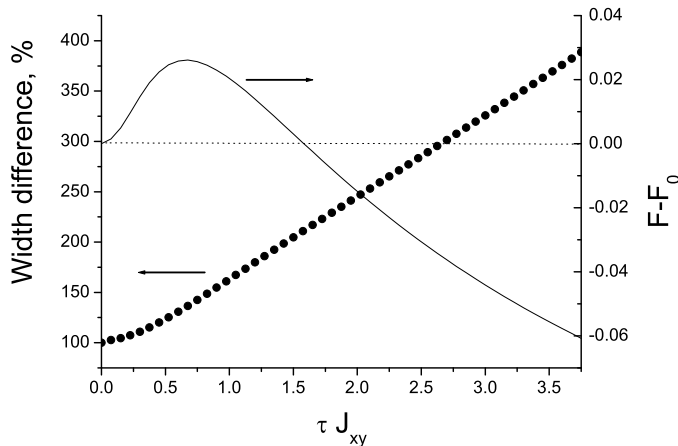


Figure 45: Dots: relative increase of the width of the first fidelity maximum in Fig. 45. Solid line: fidelity of the maximum compared to F_0

Figure 44 shows the fidelity of the state transfer after completely decoupling the last qubit from the rest of the chain for $t \rightarrow \infty$ as a function of the parameters τ and t_f (for $t_i = 0$). There is a region where the fidelity for the localized state is higher than in the time-independent case (up to 4%).

The origin of this phenomenon is similar to the effect described in Ref. [27]. By dynamically varying the coupling constant between the first and the second qubit, the information about the state enters the chain as a wave packet that has small dispersion. This corresponds to some sort of filtering, an interpretation in agreement with the fact that the fidelity is higher in the case of equal “profiles” for the coupling and decoupling functions. If we use dynamical decoupling only at the end of the chain and employ instant coupling to initialize the chain, the maximal possible fidelity for the chain of $N = 10$ qubits drops from about 0.99 to 0.95 (but it is still higher than the fidelity for the time-independent case, which is around 0.93). Apparently, during the dynamical decoupling, the information that is still dispersed in the chain will arrive at the last qubit. Therefore, slow decoupling allows more information to be gathered before the full decoupling occurs.

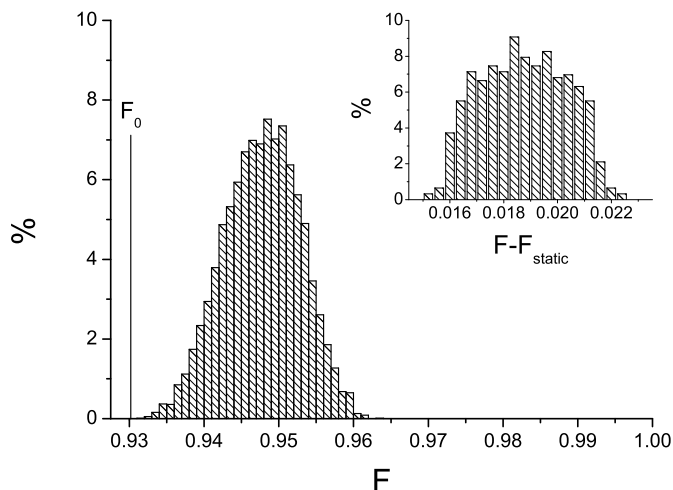


Figure 46: Fidelity distribution in the presence of small disorder in the coupling constants J_{xy} , $N = 10$, $t_i = 0$, $\tau = 0.325/J_{xy}$, $t_f = 6.2/J_{xy}$. F_0 is the first fidelity maximum for the ideal chain with static coupling constants. Inset: distribution of the fidelity difference between the dynamical and static cases in the presence of equal disorder.

One may think that we simply replace the time scale when fidelity is big in usual communication protocol by about the same time scale when we have to start decoupling procedure to achieve big fidelity. However there are two facts that make dynamical coupling constants more suitable for practical purposes. First of all, as one can see in Figures 44 and 45, adiabatic coupling requires less precise definition of t_f to achieve the same quality of the state transfer, compared to instantaneous coupling. Also it is easier to realize precise pulses of flux/voltage for coupling/decoupling instead of performing complex qubit manipulations in a very limited time scale, for example applying quantum error correction and then executing some quantum algorithm with the transmitted state.

Since we are discussing practical realization of the state transfer using spin chains, we have to take into account that experimental qubit arrays are always inhomogeneous. Therefore in the rest of the chapter we will discuss the effect of static dis-

order in J_{xy} and dynamical fluctuations in the coupling/decoupling functions. For charge qubit arrays, the most important source of inhomogeneity is the variance of the Josephson energies of the junctions (about 5%). In the case of the flux-qubit chain with capacitive coupling, J_{xy} is a complicated function of the Josephson and charging energies as well as the capacitance of the coupling capacitor, see Ref. [37]. A rough estimate using realistic parameters leads to the variance of 10%.

We have performed numerical simulations to evaluate the time evolution of the system. As a result we find out that the phenomena described above, are stable to static disorder and dynamical fluctuations in the coupling functions, see Figs. 46, 47. Figure 46 shows the distribution of the fidelity after complete decoupling in the presence of disorder in the coupling constants. Its half-width is quite small: even in the worst case the fidelity is higher than the fidelity of the ideal chain without disorder. The graph was constructed using a numerical simulation for the ensemble of 10000 chains where the coupling constants were of the form $J_{xyi} \rightarrow J_{xyi}(1 + r_i)$, $i = 1..N$. The quantity r_i was a random number with uniform distribution in the interval $[0; 0.07]$.

The inset of Fig. 46 shows the difference between the fidelities for different realizations of the chains with constant and time-dependent couplings. This difference is around 2%, so the effect of increased fidelity persists. In each realization both chains have the same randomized coupling constants and the only difference is that J_{xy1} and J_{xyN} are not multiplied by coupling functions for the time-independent chain.

Figure 47 shows the influence of fluctuations in the coupling/decoupling functions. Here the coupling constants J_{xy} are the same for all realizations and the coupling/decoupling functions are of the form

$$\begin{aligned} J_{xy1}(t) &= J_{xy} \left(1 + \exp \frac{t_i - t}{\tau} \right)^{-1} (1 + r_1(t)) \\ J_{xyN}(t) &= J_{xy} \left(1 + \exp \frac{t - t_f}{\tau} \right)^{-1} (1 + r_N(t)) . \end{aligned} \tag{91}$$

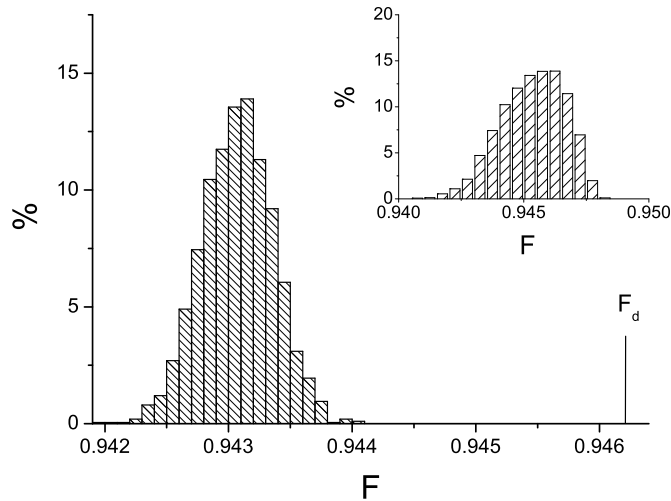


Figure 47: Fidelity distribution in the presence of fluctuations in the coupling/decoupling function, all other coupling constants are fixed and equal. $t_i = 0$, $\tau = 0.325/J_{xy}$, $t_f = 6.2/J_{xy}$. F_d is the fidelity after decoupling in the absence of fluctuations. Inset: fidelity distribution in the presence of site energy fluctuations ($\delta B = 5\%$).

The quantities $r_{1,N}(t)$ are stepwise stochastic processes of step width 0.036τ , the step heights are uniformly distributed in the interval $[0; 0.02]$. The influence of these fluctuations is small. The fidelity in the presence of dynamical fluctuations in the coupling functions is always decreased. This is in agreement with the filtering idea described above.

The inset of Fig. 47 shows the influence of fluctuations in the site energies. This influence is small, because assuming that B is chosen to maximize the average fidelity, the fluctuations of B will influence only one term in the fidelity as a multiplicative factor that is approximately equal $\cos(\delta B)$, see [8].

Finally, to check that all the effects described above are not the consequence of our special choice of coupling functions (89), we also did the calculation for another type of dynamical coupling/decoupling:

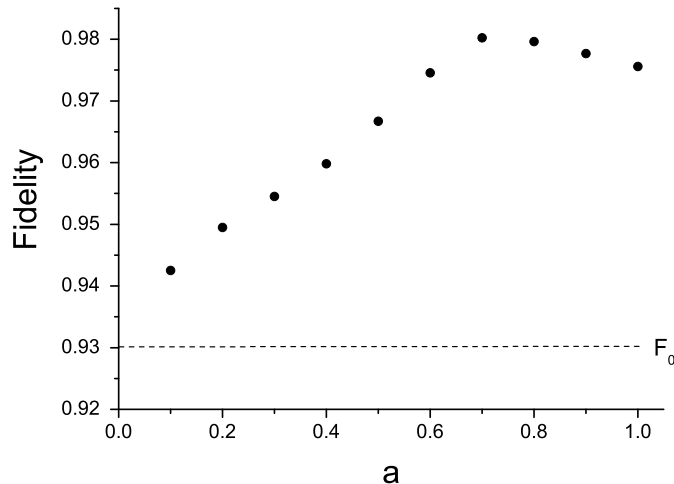


Figure 48: Fidelity maxima in the case of coupling functions parameterized as $J_{xy}((t)/\tau)^a$, $J_{xy}((t_f - t)/\tau + 1)^a$.

$$J_{xy1} = \begin{cases} 0 & t < 0 \\ J_{xy}(t/\tau)^a & t \in [0, \tau] \\ J_{xy} & t > \tau \end{cases} \quad (92)$$

$$J_{xyN} = \begin{cases} J_{xy} & t < t_f \\ J_{xy}((t_f - t)/\tau + 1)^a & t \in [t_f, t_f + \tau] \\ 0 & t > t_f + \tau \end{cases} \quad (93)$$

These functions vary from 0 to J_{xy} (and vice versa), and we have chosen $t_i = 0$. The parameters a and τ describe the shape and timescale of the coupling/decoupling function. The first maxima of the fidelity for different $a \in [0.1; 1]$ are shown in Fig. 48. Here, as in Fig. 47, τ and t_f are chosen to maximize the fidelity. One can see that this type of dynamical coupling also allows us to have better state transfer than for the chain with constant couplings (where the height of the first maximum is F_0). In general, wave packets with bigger width have lower dispersion. Therefore we expect that every smooth monotonic coupling/decoupling function with equal profiles will

allow us to improve the fidelity of state transfer.

5.3 Conclusion

In the past, a number of quantum transmission line systems was proposed to achieve a perfect or almost perfect state transfer. A common disadvantage of most of these proposals is the very short time interval, for which the fidelity of the state transfer is high. Manipulating the state in such short time intervals is impossible using current experimental technology. In this chapter we have proposed the method that allows to localize the transferred state on the last qubit of the transmission line, by varying the coupling constants between the first and last pair of qubits. We have also shown that this method increases the fidelity of the state transfer and that this effect is stable to static disorder in the coupling constants and dynamical fluctuations in the coupling/decoupling functions. We would also like to mention, that applying a sequence of coupling/decoupling pulses may lead to an even better fidelity [64].

6 Quantum interference in the state transfer via spin chains

6.1 Introduction

As with any task in quantum information processing which offers an advantage over classical information processing, the question arises what in the quantum world allows for that advantage. It is generally acknowledged that quantum entanglement and interference are two ingredients which distinguish quantum information processing from its classical counterpart [65]. Quantum entanglement has been studied in great detail over the last fifteen years [66], but the precise role of interference in various quantum information treatment tasks remains to be elucidated [67].

Contrary to entanglement, interference is a property not of a quantum state but of the propagator of a state. This is due to the fact that the coherence of the propagation is important for interference. Indeed, the final probability distribution resulting from a given quantum algorithm can always be generated through stochastic simulation on a classical computer as well: for a known quantum circuit and initial state one can, in principle, calculate the final state, and, therefore, the probability distribution. It is then simple to create a stochastic process which gives each possible outcome with the correct probability. In such a classical simulation clearly no interference takes place. Thus, what counts for interference is not a state itself but the way it was created.

A quantitative measure of interference in any quantum mechanical process in a finite-dimensional Hilbert space was recently introduced in [68], and the statistics of quantum interference in random quantum algorithms was studied in [69]. Here we propose to study the role of interference in quantum state transfer through spin chains. After defining the notion of interference, reduced interference, and fidelity in Subsection 6.3.1, we will follow two complementary approaches: in Subsection 6.3.2 we will consider the spin chain as a black box which propagates the initial state of the

first and last spins combined to a final state of these two spins. We will calculate the reduced interference that describes this propagation for different spin chains and show that perfect state transfer is possible without quantum interference. In Subsection 6.3.5 we will then consider the unitary evolution of the entire chain and analyze this unexpected result.

6.2 Quantum interference

The quantity, that quantify the amount of interference present in any physical process that maps an initial density matrix to a final density matrix was introduced in [68]. This quantity, called quantum interference, is connected to several phenomena that capture the essence of its classical counterpart [68]:

1. Coherence. As in classical case, quantum interference should be able to distinguish between coherent and incoherent propagation. That's why it was mentioned earlier that measure of interference is a property of the propagator of states.
2. Equipartition. If propagator just permutes incoming amplitudes, there is no interference involved. Interference requires coherent superposition of several states and therefore its measure should be linked to how many different initial state amplitudes contribute to each final state amplitude and to what extent. This measure should be maximal if each basis state as input produce an equipartitioned output state, i.e. state with the same absolute probability amplitude for each basis state.
3. Basis dependence. Interference measure should depend on basis in which the propagator matrix is described. Like in classical double slit experiment there is no interference pattern if we observe it in the momentum basis.

Taking into account these three phenomena the interference $I(t)$ for a general quantum process described by a propagator $\mathcal{P}(t) = P_{ij,kl}(t)$ which propagates an initial state ρ with matrix elements ρ_{ij} in a fixed orthonormal basis of dimension D to a final state ρ' ,

$$\rho'_{ij} = \sum_{k,l=1}^D P_{ij,kl} \rho_{kl} \quad (94)$$

is defined as [68]

$$I(t) = \sum_{i,k,l} |P_{ii,kl}(t)|^2 - \sum_{i,k} |P_{ii,kk}(t)|^2. \quad (95)$$

6.3 Role of quantum interference in the state transfer

6.3.1 Interference and reduced interference

If \mathcal{P} describes the propagation of the reduced density matrix of the first and last spins alone (which will be mixed in general, as it results from tracing out the intermediate spins of the chain), Eq. (95) defines the “reduced interference” $I_r(t)$. We will evaluate $I_r(t)$ analytically for spin chains which conserve the number of excitations in the chain, and show that $I_r(t)$ is intimately linked to the average fidelity $F(t)$,

$$F(t) = \frac{1}{4\pi} \int \langle \psi_{in} | \rho_{out}(t) | \psi_{in} \rangle d\Omega, \quad (96)$$

where $|\psi_{in}\rangle$ is the pure state to be transmitted prepared on the first spin, ρ_{out} is the output state on the last spin (i.e. $\rho_{out} = \text{Tr}_1 \rho'$, with the trace over the first (input) spin), and the integral is over all initial states of the input spin on the Bloch sphere parameterized by the spatial angle Ω . We will also provide numerical results for $I_r(t)$ for chains in which the number of excitations is not conserved.

The interference measure for unitary propagation of the entire chain, $|\psi'\rangle = U|\psi\rangle$

reduces to [68]

$$I_U(t) = D - \sum_{i,k=1}^D |U_{i,k}(t)|^4. \quad (97)$$

For this coherent propagation, the interference $I_U(t)$ measures the degree of equipartition of the output that result from any basis state of a system at $t = 0$. Here, an equipartitioned state means a state that is a superposition of all the basis states with amplitudes of modulus $1/\sqrt{D}$. For better comparison of the results we will plot the normalized interference $I = I_U/(D - 1)$ so that the maximal possible value of the interference is one and does not depend on the number of qubits in the chain.

6.3.2 Reduced interference for excitation-conserving spin chains

We start by evaluating the reduced interference in excitation-preserving chains, i.e., spin chains for which the total Hamiltonian H commutes with the total spin component $S^z = \sum_{i=1}^N \sigma_i^z$. The particular example of the chain with isotropic Heisenberg interaction proposed by Bose [8] falls into this class (see Section 6.3.3 below). We start with at most one excitation in the chain and limit ourselves to pure initial states. Therefore one can specify a state of the entire chain $|j\rangle$ ($j = 1, \dots, N$) by the position at which the excitation is localized. In principle there are four computational basis states for the two spins, but the state where both the first and last spins are excited will never appear. We therefore restrict our attention to the three-dimensional Hilbert space spanned by the states $|1\rangle$, $|N\rangle$, and $|0\rangle_r$ (the state where both the first and last spins are not excited). We will also make use of the state $|0\rangle_m$ of the intermediate part of the chain, where all intermediate spins are not excited.

We start from an initial state of the chain which factorizes between the two selected spins (1 and N) and the rest of the chain, which is assumed to be in state $|0\rangle_m$,

$$|\Psi_{in}\rangle = (a_0|0\rangle_r + a_1|1\rangle + a_N|N\rangle)|0\rangle_m. \quad (98)$$

The initial reduced density matrix of the first and last spins,

$$\rho = \begin{pmatrix} |a_0|^2 & a_0 a_1^* & a_0 a_N^* \\ a_1 a_0^* & |a_1|^2 & a_1 a_N^* \\ a_N a_0^* & a_N a_1^* & |a_N|^2 \end{pmatrix}, \quad (99)$$

then still represents a pure state. For any Hamiltonian that conserves the number of excitations we can write the state at time t as

$$|\Psi_{out}(t)\rangle = a_0 |0\rangle_r |0\rangle_m + a_1 \sum_{j=1}^N \langle j | e^{-iHt} |1\rangle |j\rangle + a_N \sum_{j=1}^N \langle j | e^{-iHt} |N\rangle |j\rangle, \quad (100)$$

or

$$\begin{aligned} |\Psi_{out}(t)\rangle = & a_0 |0\rangle_r |0\rangle_m + a_1 f_{11} |1\rangle |0\rangle_m + a_1 \sum_{j=2}^{N-1} \langle j | e^{-iHt} |1\rangle |0\rangle_r |j\rangle + \\ & a_1 f_{N1} |N\rangle |0\rangle_m + a_N f_{1N} |1\rangle |0\rangle_m + a_N \sum_{j=2}^{N-1} \langle j | e^{-iHt} |N\rangle |0\rangle_r |j\rangle + a_N f_{NN} |N\rangle |0\rangle_m, \end{aligned} \quad (101)$$

where

$$f_{ij}(t) = \langle i | e^{-iHt} |j\rangle. \quad (102)$$

After tracing out the intermediate spins we obtain the final density matrix of the first and last spins,

$$\rho' = \begin{pmatrix} |a_0|^2 + S_m & a_0(a_1^* f_{N1}^* + a_N^* f_{NN}^*) & a_0(a_1^* f_{11}^* + a_N^* f_{1N}^*) \\ a_0^*(a_1 f_{N1} + a_N f_{NN}) & |a_1 f_{N1} + a_N f_{NN}|^2 & (a_1 f_{N1} + a_N f_{NN})(a_1^* f_{11}^* + a_N^* f_{1N}^*) \\ a_0^*(a_1 f_{11} + a_N f_{1N}) & (a_1 f_{11} + a_N f_{1N})(a_1^* f_{N1}^* + a_N^* f_{NN}^*) & |a_1 f_{11} + a_N f_{1N}|^2 \end{pmatrix} \quad (103)$$

where

$$S_m = \sum_{j=2}^{N-1} |a_1 \langle j | e^{-iHt} |1\rangle + a_N \langle j | e^{-iHt} |N\rangle|^2. \quad (104)$$

Comparing Eqs. (99), (103), and (94) we read off the propagator

$$\mathcal{P} = \begin{pmatrix} 1 & 0 & 0 & 0 & \sum_j |f_{j1}|^2 & \sum_j f_{j1}f_{jN}^* & 0 & \sum_j f_{jN}f_{j1}^* & \sum_j |f_{jN}|^2 \\ 0 & f_{N1}^* & f_{NN}^* & 0 & 0 & 0 & 0 & 0 & 0 \\ 0 & f_{11}^* & f_{1N}^* & 0 & 0 & 0 & 0 & 0 & 0 \\ 0 & 0 & 0 & f_{N1} & 0 & 0 & f_{NN} & 0 & 0 \\ 0 & 0 & 0 & 0 & |f_{N1}|^2 & f_{N1}f_{NN}^* & 0 & f_{NN}f_{N1}^* & |f_{NN}|^2 \\ 0 & 0 & 0 & 0 & f_{N1}f_{11}^* & f_{N1}f_{1N}^* & 0 & f_{NN}f_{11}^* & f_{NN}f_{1N}^* \\ 0 & 0 & 0 & f_{11} & 0 & 0 & f_{1N} & 0 & 0 \\ 0 & 0 & 0 & 0 & f_{11}f_{N1}^* & f_{11}f_{NN}^* & 0 & f_{1N}f_{N1}^* & f_{1N}f_{NN}^* \\ 0 & 0 & 0 & 0 & |f_{11}|^2 & f_{11}f_{1N}^* & 0 & f_{1N}f_{11}^* & |f_{1N}|^2 \end{pmatrix}, \quad (105)$$

where the rows and columns are in the order 00, 01, 0N, 10, 11, 1N, N0, N1, NN.

Inserting \mathcal{P} into Eq. (95), we obtain

$$I_r(t) = \left| \sum_{j=2}^{N-1} \langle j | e^{-iHt} | 1 \rangle \langle N | e^{iHt} | j \rangle \right|^2 + \left| \sum_{j=2}^{N-1} \langle j | e^{-iHt} | N \rangle \langle 1 | e^{iHt} | j \rangle \right|^2 \\ + |f_{N1}f_{NN}^*|^2 + |f_{NN}f_{N1}^*|^2 + |f_{11}f_{1N}^*|^2 + |f_{1N}f_{11}^*|^2 \quad (106)$$

for the reduced interference. This expression can be further simplified by using

$$\sum_{j=1}^N \langle N | e^{iHt} | j \rangle \langle j | e^{-iHt} | 1 \rangle = \langle N | 1 \rangle = 0, \quad (107)$$

such that

$$I_r(t) = 2 |f_{11}f_{N1}^* + f_{N1}f_{11}^*|^2 + 2 |f_{11}f_{1N}^*|^2 + 2 |f_{N1}f_{NN}^*|^2. \quad (108)$$

This result is valid for any Hamiltonian of the entire chain that conserves the number of excitations. In the case of a linear chain with symmetrical nearest-neighbor inter-

actions (i.e. the Hamiltonian is invariant under relabeling the qubits $1, 2, \dots, N$ into $N, \dots, 2, 1$), we have $f_{1N} = f_{N1}$ and $f_{11} = f_{NN}$. The reduced interference can then be expressed using two amplitudes of the state transfer,

$$\begin{aligned} I_r(t) &= 8|f_{11}|^2|f_{1N}|^2 + 2f_{11}^2(f_{1N}^*)^2 + 2f_{N1}^2(f_{11}^*)^2 \\ &= 4|f_{11}|^2|f_{1N}|^2(1 + 2\cos^2(\gamma_{11} - \gamma_{1N})), \end{aligned} \quad (109)$$

where $\gamma_{ij} = \arg(f_{ij})$. We are now in the position to evaluate $I(t)$ for specific examples.

6.3.3 Chains that conserve the number of excitations

Let us first consider the spin chains studied in [8] and described in the introduction part of this thesis. They consist of a one-dimensional array of N spins, with nearest-neighbor spins coupled through an isotropic Heisenberg interaction. The Hamiltonian of the chain reads

$$H = - \sum_{i=2}^N J \boldsymbol{\sigma}_i \cdot \boldsymbol{\sigma}_{i-1} - \sum_{i=1}^N B_i \sigma_i^z, \quad (110)$$

where $\boldsymbol{\sigma}_i = (\sigma_i^x, \sigma_i^y, \sigma_i^z)$ denotes the vector of the Pauli matrices on site i , B_i denotes the site-dependent static magnetic field and $J > 0$ is the coupling strength, taken as constant for all spins.

As was shown earlier, the average fidelity, Eq. (96), for this model is given by

$$F = \frac{|f_{1N}| \cos \gamma_{1N}}{3} + \frac{|f_{1N}|^2}{6} + \frac{1}{2}. \quad (111)$$

At $t = 0$, $f_{1N} = 0$ for $N > 1$, such that the average fidelity corresponds to the fidelity of a random guess of Bob of the quantum state of Alice ($F = 1/2$). The overlap $f_{1N}(t)$ becomes appreciable, once the spin wave excited at Alice's end arrives at Bob's spin. Perfect state transfer for all states ($F = 1$) requires $f_{1N} = 1$, along with $\cos \gamma_{1N} = 1$.

By comparing Eqs. (109) and (111) one can see that interference is determined by one more complex variable f_{11} compared to the fidelity. Therefore, in general there is no explicit formula that describes interference in terms of fidelity alone. Naively one might expect that interference should play an important role for quantum state transfer, if the fidelity of the process exceeds the maximal classical value, $F = 2/3$ [9]. However, note that an ideal quantum state transfer can be realized through the permutation of the first and last spins $|0\rangle_r \leftrightarrow |0\rangle_r$, $|1\rangle \leftrightarrow |N\rangle$, which does not lead to any interference at all. In general, interference measures both the equipartition of all output states for any computational basis state as input, and the coherence of the propagation. “Coherence” was defined in [68] as the sensitivity of the final probabilities ρ'_{ii} to the initial phases. As is evident from Eq. (109), the only phase information which contributes to the reduced interference in the propagation through the spin chain is the relative phase between the states $|0\rangle_r$ and $|N\rangle$. However, the coherence of the propagation becomes irrelevant for perfect transfer, $f_{1N} = 1$, as then $f_{NN} = 0$ due to conservation of the number of excitations, and then the final probabilities do not depend on any initial phases anymore. I.e. for ideal state transfer, the dynamics of the chain indeed realizes the above permutation with vanishing interference. This is also evident from Eq. (109) for $f_{11} = f_{NN} = 0$. Note, however, that the interference is finite during the propagation of the signal through the chain, as well as quite generally for any situation in which neither f_{11} nor f_{1N} vanish. All one can say is that for $F(t)$ close to 1, i.e. f_{1N} close to 1 and thus f_{NN} close to 0 - $I_r(t)$ remains quite small. We would also like to mention, that in a simple series of swap (SOS) protocol the reduced interference for chains with more than two qubits is always zero, since either f_{11} or f_{1N} has zero value at any time.

Figure 49 shows $I_r(t)$ that was obtained by numerically propagating $|\Psi(t)\rangle$ for $N = 20$ (see Eq. (100)) with the Hamiltonian (110). The results are plotted with time in units of $1/J$. We also assumed that $B_i = B$ for all i , and therefore the

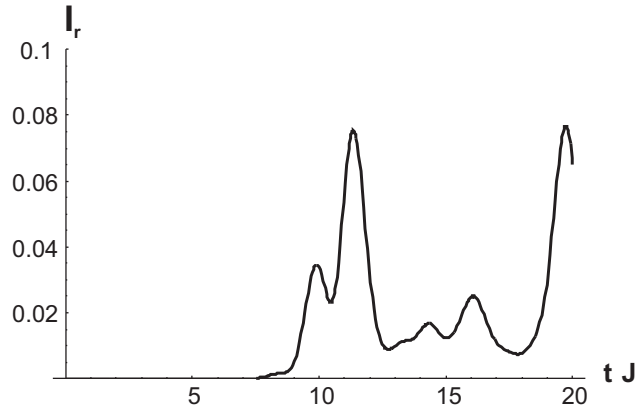


Figure 49: Reduced interference for a spin chain with $N = 20$ qubits described by the model defined in Eq. (110).

interference does not depend on magnetic field. Indeed, in our model B influences only the phases of f_{11} and f_{1N} through a term $\exp(-2iBt)$ (see, for example [8]) and according to Eq. (109) the interference depends only on phase differences and not on a global phase. One can see that the interference remains quite small. This is because the probability to find an excitation inside the chain is high and both quantities $|f_{11}|^2$ and $|f_{1N}|^2$ cannot be big (~ 0.5) at the same time at the time scale that is relevant for quantum state transfer.

Let us now consider the case of reduced coupling constants of spins 1 and N to the rest of the chain

$$H = - \sum_{i=2}^N J_i (\sigma_i^x \sigma_{i-1}^x + \sigma_i^y \sigma_{i-1}^y), \quad (112)$$

with $J_2 = J_N = aJ$ where $a \ll 1$, and $J_{i \neq 2, N} = J$. It was shown in [24] that this can drastically increase the fidelity of the state transfer. Figure 50 shows the reduced interference $I_r(t)$ together with $F(t)$. We see that both are perfectly anticorrelated. In particular, we have again $I_r(t) \simeq 0$ for $F(t) \simeq 1$ for the same reasons as discussed before. The interference is maximal half way through the perfect state transfer. In this case, the interference is not small (compare Fig. 49 and Fig. 50) since due to the weak coupling the intermediate spins are only slightly excited [24] and both quantities

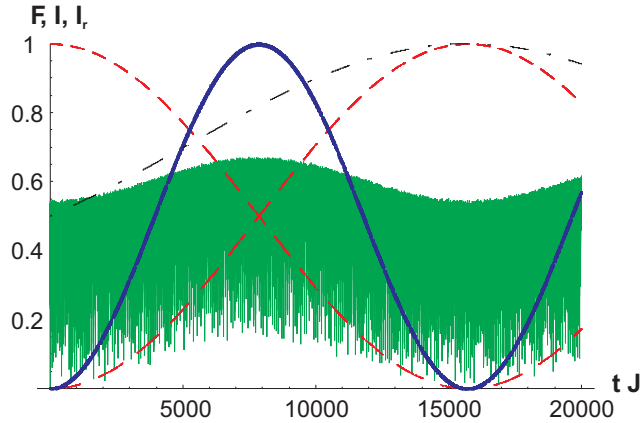


Figure 50: Reduced interference I_r for the case of small coupling constants between the first and the last pair of qubits, $N = 8$ (blue, thick solid line). The green (thin solid) line shows the full interference of the entire chain (renormalized by a factor $1/N$). The black (dot-dashed) line shows the fidelity $F(t)$. The red (dashed) lines are the probabilities to find an excitation on the first qubit and on the last qubit ($|f_{11}|^2$ and $|f_{1N}|^2$, respectively) if we start with the excitation on the first qubit.

f_{11} and f_{1N} can be big ($1/\sqrt{2}$) at the same time (see red (dashed) curves in Fig. 50).

6.3.4 Chains that do not conserve the number of excitations

Now we consider a more general Hamiltonian that does not conserve the number of excitations,

$$\begin{aligned}
 H &= - \sum_{i=2}^N [J_{xy}(\sigma_i^x \sigma_{i-1}^x + \sigma_i^y \sigma_{i-1}^y) + J_z \sigma_i^z \sigma_{i-1}^z] \\
 &\quad - \sum_{i=1}^N (\Delta \sigma_i^x + B \sigma_i^z).
 \end{aligned} \tag{113}$$

Equation (113) is a more realistic model than Eq. (110) since in real qubits the σ^x term, which describes the tunneling between the states $|0\rangle$ and $|1\rangle$, cannot always be neglected. A physical realization of Hamiltonian (113) was proposed in [62]. Sometimes the σ^x term can be suppressed [38, 62], but for longer chains even small values of Δ will influence the dynamics of the chain. In this case, Eq. (109) is not valid anymore, and the question of how much interference is used in the quantum state

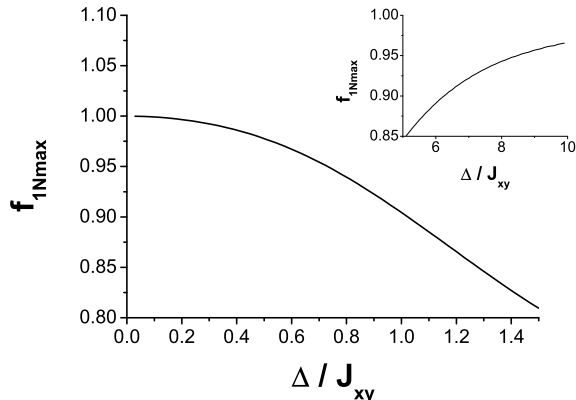


Figure 51: Global maxima of $f_{1N} = \langle 1|e^{-iHt}|N \rangle$ in the time interval $[0, 1/J_{xy}]$ as a function of Δ for the model defined by Eq. (113), $N = 3$.

transfer needs to be reassessed. Since the number of excitations is not conserved, we have to do the calculation in the much larger Hilbert space with dimensionality 2^N instead of $N + 1$. One can numerically evaluate $\rho'(t)$ and find $I_r(t)$ as a function of time. We used realistic qubit parameters that are typical for flux qubits, see [37, 62], namely $J_{xy} = 0.08J_z$, and $B = 0$. The results of the calculations are shown in Figs. 51 and 52.

Figure 51 shows the global maxima of $f_{1N} = \langle 1|e^{-iHt}|N \rangle$ in the time interval $[0, 1/J_{xy}]$ as a function of Δ for a chain with $N = 3$ qubits. The quantity f_{1N} decreases with Δ until the time required for the state to be transferred from the first to the last qubit is approximately equal to $1/\Delta$. This is in agreement with [62]. For large Δ , f_{1N} is close to one due to excitations that are created in the chain during this time interval.

Figure 52 shows the reduced interference at the global maxima of $f_{1N} = \langle 1|e^{-iHt}|N \rangle$ in the time interval $[0, 1/J_{xy}]$. Once again, interference decreases with increasing f_{1N} , and vice versa, but this time as a function of the parameter Δ . For very small Δ , we have nearly perfect state transfer (almost no equipartition and coherence), therefore the interference is small. It increases with Δ , as the creation of excitations enhances

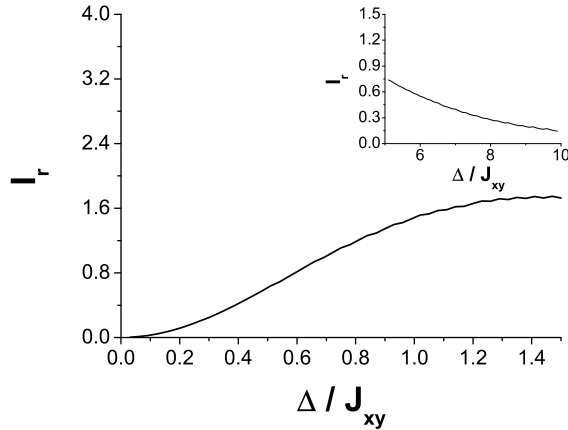


Figure 52: Reduced interference at the global maxima of $f_{1N} = \langle 1|e^{-iHt}|N\rangle$ in the time interval $[0, 1/J_{xy}]$, see Fig. 51.

the equipartition and sensitivity of the final state to the initial state. For large Δ , when a high value f_{1N} is achieved due to excitations created in the chain, interference is small. For example if the excitation is created on the last qubit, then the amplitude $|f_{1N}|$ will be equal to one. It corresponds to nearly stochastic transfer, since the final probabilities to find the last qubit in the state $|0\rangle$ or $|1\rangle$ are almost independent of the initial state.

6.3.5 Interference in the unitary propagation of the entire chain

The result that perfect quantum state transfer is possible (and realized!) without quantum interference is rather counter-intuitive. It is natural to wonder what happens within the chain. Let us therefore open the black box and study the interference in the propagation of the state of the entire chain (called “full interference” $I = I_U/(D-1) = I_U/N$ in the following, where confusion is possible) for chains which conserve the number of excitations. This corresponds to a unitary propagation, and we will therefore employ Eq. (97) to quantify the interference.

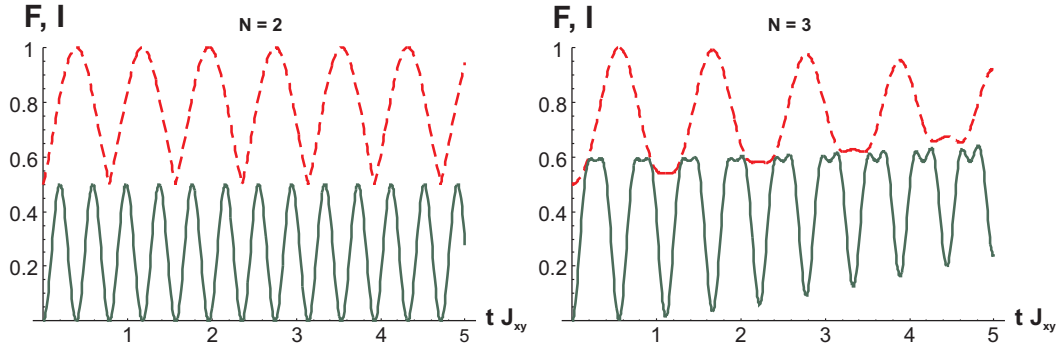


Figure 53: Fidelity (red, dashed line) and normalized full interference (green, solid line) for $N = 2$ and $N = 3$ qubits with uniform coupling constants, Eq. (114).

Chain with uniform coupling constants

For a simple chain that consists of more than three qubits, the fidelity is always less than one (except the case of specially engineered coupling constants). This is due to the fact, that the input state gets dispersed over the spins at all times $t > 0$.

Using the theory described in [62] we calculated the eigenstates and the eigenenergies of a more general version of the Hamiltonian (110),

$$H = - \sum_{i=2}^N [J_{xy}(\sigma_i^x \sigma_{i-1}^x + \sigma_i^y \sigma_{i-1}^y) + J_z \sigma_i^z \sigma_{i-1}^z] - \sum_{i=1}^N B \sigma_i^z. \quad (114)$$

This Hamiltonian also conserves the number of excitations and describes the chains of superconducting qubits, proposed in [62] and [61]. Knowing the eigenvalues and eigenenergies of (114) allows us to find the matrix elements U_{ik} and numerically calculate the full interference as a function of time and of the number of the qubits in the chain, restricting ourselves again to the $(N + 1)$ -dimensional Hilbert space of the states in Eq. (98). The results of these calculations are shown in Figs. 53, 54 for $J_z/J_{xy} = 0.05$ [62].

As we can see in Fig. 53, the full interference is close to zero if the fidelity is

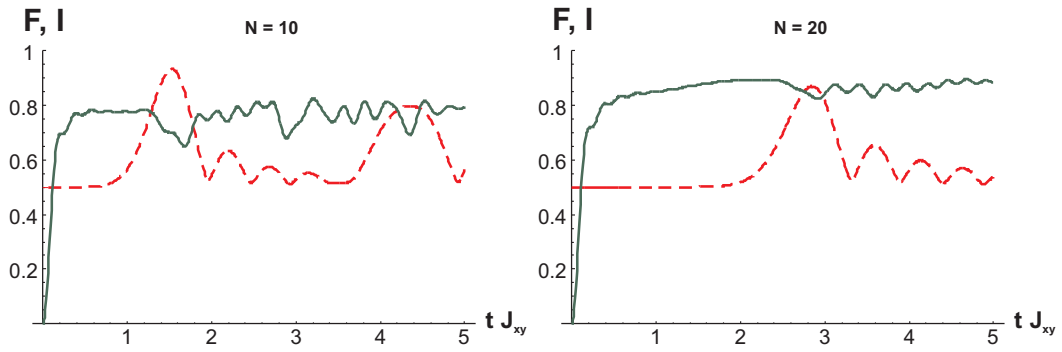


Figure 54: Fidelity (red, dashed line) and normalized full interference (green, solid line) for $N = 10$ and $N = 20$ qubits with uniform coupling constants, Eq. (114).

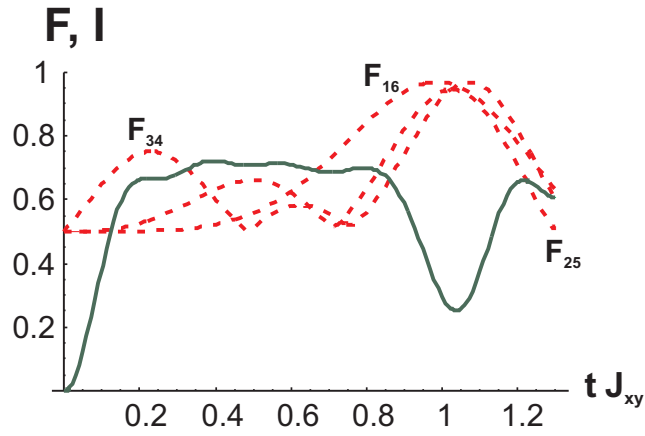


Figure 55: Fidelities (red, dashed line) and normalized full interference (green, solid line) for $N = 6$ qubits with uniform coupling constants, Eq. (114).

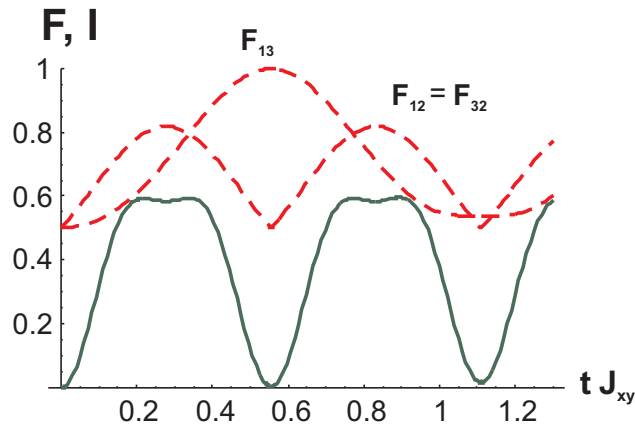


Figure 56: Fidelities (red, dashed line) and normalized full interference (green, solid line) for $N = 3$ qubits with uniform coupling constants, Eq. (114).

close to one. The reason is that the time that is required for the excitation to be transferred from the first to the last qubit (the time of the first fidelity maximum) is approximately equal to the time that it takes for the excitation to travel from qubit 2 to the end of the chain and then back to qubit $N-1$ (and so on). This is illustrated in Fig. 55, where the fidelities $F_{ij} = \frac{|f_{ij}|}{3} + \frac{|f_{ij}|^2}{6} + \frac{1}{2}$ and the normalized full interference are shown for the chain of $N = 6$ qubits. We can see that the interference is minimal in the region where local maxima of the fidelities are located. When all maxima are close to one, then, independently of the initial state, the final state will have small equipartition and therefore the interference is small.

When the fidelity maximum goes down, the corresponding full interference increases rapidly (see, for example, Fig. 53, $N = 3$). Hence, I is very sensitive to the amplitude distribution of the final state over the qubits. Here the amplitude of the spin j in the final state is $f_{1j} = \langle 1 | e^{-iHt} | j \rangle$.

For short chains the fidelity maxima correspond to minimal dispersion. For longer chains, the minima of the full interference are shifted with respect to the fidelity maxima. This is due to the fact that a maximal amplitude of the state “up” of the last qubit does not necessarily correspond to the minimal dispersion as measured by interference, which takes into account all possible input states.

Another feature of the interference graph are intermediate minima which correspond to a partial localization of the excitation on the intermediate qubits. For example in Fig. 53 ($N = 3$) there are clear shallow local interference minima that correspond to localization of the excitation on the nearest neighbor of the initial qubit, see Fig. 56. Deep minima correspond to localization of the excitation after the state is transferred through the whole chain. For longer chains, the times when the excitation is localized on intermediate qubits depends on the initial state, i.e. the fidelity maxima do not exactly coincide (see Fig. 55). Therefore these small features are less pronounced.

Reduced coupling constants at the end of the chain

The full (normalized) interference $I(t)$ for a chain with reduced coupling constants between the first and last pair of qubits is shown as the green solid line in Fig. 50. $I(t)$ oscillates rapidly on the time scale of the state transfer from the first to the last qubit, with an envelope whose upper boundary perfectly correlates with the oscillations of the reduced interference and an amplitude which is, for $N = 8$, about a tenth of the amplitude of the reduced interference $I_r(t)$. This behavior is indeed to be expected from the fact that $I(t)$ is a sum of equipartition measures for all initial states localized on any qubit in the chain, whereas $I_r(t)$ measures equipartition only on the first and last qubits. As the state transfer is basically perfect (and therefore $I_r(t) = 0$ for $t = 0$ and at the time of optimal transfer $t = t_1$), the lack of this contribution to the equipartition measure leads to a minimum in the envelope of $I(t)$ at $t = 0$ and $t = t_1$. At the same time, the maximum of the envelope of $I(t)$ halfway through the state transfer (corresponding to an additional contribution of about 0.1 to $I(t)$) indicates that the equipartition of the first and last qubit captures the essence of the equipartition in the chain for an initial state localized on the first qubit. This agrees with Ref. [24] since there is only a small amplitude for an excitation inside the chain during the state transfer. Therefore the equipartition between the first and last qubit gives the main contribution to the full interference.

6.4 Conclusion

In summary we have calculated the interference during the transfer of a quantum state through several types of one-dimensional spin chains with time-independent nearest-neighbor coupling constants, both for chains which do or do not conserve the number of spin excitations. We have shown that for a high-fidelity transfer the

reduced interference of the propagator of just the first and last qubits is very small, and vanishes for perfect transfer. This can be understood from energy conservation and the fact that interference measures, besides phase coherence, the equipartition of the final states for all computational states taken as input states. The full interference of the entire chain (propagated unitarily) shows rapid oscillations on the time scale of a complete transfer. For a chain with reduced coupling constants between the first and last pair of qubits the envelope of these oscillations follows the reduced interference. Thus, interference is not only valuable tool for investigating quantum algorithms, but also gives us a deeper insight into the dynamics of quantum state transfer.

7 Conclusion and outlook

Controllable coupling between quantum bits and quantum state transfer between quantum bits via 'quantum wires', two main problems discussed in this thesis, are important topics in quantum information science. Many quantum computer proposals differ only in the nature of the quantum bit elemental base but repeat the classical 'gate' concept of the computing device. It naturally implies possibility to connect different gates between each other and qubits that serve as a quantum memory. Starting from controllable interqubit coupling, that is a key element for building an universal set of quantum gates, this thesis leads to the proposal for realization of the effective quantum state transfer in flux-qubit based quantum computers. The second part of this thesis is devoted to the method, that allows us to localize the transferred state and improve the fidelity of the state transfer at the same time. It can also be used as a part of other methods for achieving an effective state transfer such as different multi-rail protocols, 'quantum valve' proposal and conclusive transfer to improve their efficiency. Finally, we analyzed the role of interference measure proposed in [68] in studying quantum state transfer via spin chains.

While state transfer with quantum chains is relatively young and small part of quantum information science, it is quite active and more than hundred theoretical articles appeared in the last few years. They describe possible realizations and provide methods to increase the efficiency of the basic idea. However, no real experiments were done yet and realizing proof-of-principle state transfer in a short chain is an important goal for the nearest future. Around working experimental setup one could build system specific theories, that take into account decoherence, dephasing, noise and other system dependant phenomena that influence the efficiency of the state transfer.

Appendix A. Calculation of the fidelity using software *Mathematica 5.2*

All the numerical calculations in this thesis were performed by using mathematical software system *Mathematica 5.2*. To calculate the fidelity for figures in introduction and chapters 3-6 we used the qubit parameters that are specific for persistent-current qubits [37, 36] and formulas (65), (72) and (73). Most of the results were plotted in dimensionless units, where time was measured in the inverse energies that characterize qubits or coupling between them. Therefore most of our results depend only on the form of the Hamiltonian and the ratio of energies that characterize it. Typical block-scheme of fidelity calculation for ideal XXZ -Hamiltonian (88) was as follow:

1. Hamiltonian parameters are initialized in units of energy, that characterize either qubits (usually Josephson energy E_J) or coupling between them (usually J_{xy}).
2. Equation (82) was solved numerically using built-in Mathematica function *Solve[]*.
3. Arrays of eigenenergies and eigenvalues of the Hamiltonian were formed using equations (81), (84) and (86).
4. Fidelity was calculated using equations (77) and (87).
5. To determine the maxima of the fidelity as function of time, we use a discretization step of $0.01/J_{xy}$. This is enough to give us the maxima and the time when they are achieved with a sufficient precision since the half-width of the maximum profile is in the order of $1/J_{xy}$.

References

- [1] R. Beals, H. Buhrman, R. Cleve, M. Mosca and R. de Wolf, quant-ph/9802049.
- [2] D. P. DiVincenzo, Fortsch. Phys. **48**, 771 (2000).
- [3] L. M. K. Vandersypen, M. Steffen, G. Breyta, C. S. Yannoni, M. H. Sherwood and I. L. Chuang, Nature **414**, 883887 (2001).
- [4] D. P. DiVincenzo, Phys. Rev. A **51**, 1015 (1995).
- [5] A. Barenko, C. H. Bennett, R. Cleve, D. P. DiVincenzo, N. Margolus, P. Shor, T. Sleator, J. A. Smolin and H. Weinfurter, Phys. Rev. A **52**, 3457 (1995). (1995).
- [6] R. Raussendorf and H.-J. Briegel, Phys. Rev. Lett. **86**, 5188 (2001).
- [7] R. Raussendorf, R. D. Browne and H.-J. Briegel, Phys. Rev. A **68**, 022312 (2003).
- [8] S. Bose, Phys. Rev. Lett. **91**, 207901 (2003).
- [9] M. Horodecki, P. Horodecki and R. Horodecki, Phys. Rev. A **60**, 1888 (1999).
- [10] W. K. Wootters and W. H. Zurek, Nature **299**, 802 (1982).
- [11] Knill, quant-ph/0410199v2, (2004).
- [12] M. Christandl, N. Datta, A. Ekert, and A. J. Landahl, Phys. Rev. Lett. **92**, 187902 (2004).
- [13] M. Paternostro, G. M. Palma, M. S. Kim, and G. Falci, Phys. Rev. A **71**, 042311 (2004).
- [14] P. Karbach and J. Stolze, Phys. Rev. A **72**, 030301(R) (2005).
- [15] G. M. Nikolopoulos, D. Petrosyan, and P. Lambropoulos, Europhys. Lett. **65**, 297 (2004).

- [16] S. Yang, Z. Song and C. P. Sun, Phys. Rev. B **73**, 195122 (2006).
- [17] A. Kay and M. Ericsson, New J. Phys. **7**, 143 (2005).
- [18] M. H. Yung, D. W. Leung, and S. Bose, Quant. Inf. Comp. **4**, 174 (2004).
- [19] D. Burgarth, S. Bose, and V. Giovannetti, J. Phys. A: Math. Gen. **38**, 6793 (2004).
- [20] D. Burgarth, and S. Bose, Phys. Rev. A **71**, 052315 (2005).
- [21] D. Burgarth and S. Bose, New J. Phys. **7**, 135 (2005).
- [22] T. J. Osborne and N. Linden, Phys. Rev. A **69**, 052315 (2004).
- [23] D. Burgarth, V. Giovannetti and S. Bose, Int. J. Quant. Inf. **4**, 405 (2006).
- [24] A. Wójcik, T. Łuczak, P. Kurzyński, A. Grudka, T. Gdala, and M. Bednarska, Phys. Rev. A **72**, 034303 (2005).
- [25] M.B. Plenio and F.L. Semaño, New J. Phys. **7**, 73 (2005).
- [26] Y. Li, T. Shi, B. Chen, Z. Song and C.P. Sun, Phys. Rev. A **72**, 022301 (2005).
- [27] H. L. Haselgrove, Phys. Rev. A **72**, 062326 (2005).
- [28] J. Fitzsimons and J. Twamley, Phys. Rev. Lett. **97**, 090502 (2006).
- [29] J. Fitzsimons, L. Xiao, S. C. Benjamin and J. A. Jones, Phys. Rev. Lett. **99**, 030501 (2007).
- [30] R. Raussendorf, Phys. Rev. A **72**, 052301 (2005).
- [31] C. J. Wellard, L. C. L. Hollenberg and C. I. Pakes, Nanotechnology **13**, 570 (2002).
- [32] Y. Nakamura, Yu. A. Pashkin and J. S. Tsai, Nature **398**, 786788 (1999).

- [33] I. Chiorescu, Y. Nakamura, C. J. P. M. Harmans and J. E. Mooij, *Science* **299**, 18691871 (2003).
- [34] F. Plastina, R. Fazio, and G. M. Palma, *Phys. Rev. B* **64**, 113306 (2001).
- [35] Yu. A. Pashkin, T. Yamamoto, O. Astafiev, Y. Nakamura, D. V. Averin and J. S. Tsai, *Nature* **421**, 823-826 (2003).
- [36] Mooij J E, Orlando T P, Levitov L S, Tian L, van der Wal C H and Lloyd S 1999 *Science* **285** 1036
- [37] T. P. Orlando, J. E. Mooij, L. Tian, C. H. van der Wal, L. Levitov, S. Lloyd, and J. J. Mazo, *Phys. Rev. B* **60**, 15398 (1999).
- [38] L. S. Levitov, T. P. Orlando, J. B. Majer, and J. E. Mooij, cond-mat/0108266, (2001).
- [39] J. Q. You, Y. Nakamura, and Franco Nori, *Phys. Rev. B* **71**, 024532 (2005).
- [40] J. Siewert, R. Fazio, G. M. Palma, and E. Sciacca, *J. Low Temp. Phys.* **118**, 795 (2000).
- [41] D. Vion, A. Aassime, A. Cottet, P. Joyez, H. Pothier, C. Urbina, D. Esteve, and M. H. Devoret, *Science* **296**, 886 (2002).
- [42] P. Bertet, I. Chiorescu, G. Burkard, K. Semba, C. J. P. M. Harmans, D. P. DiVincenzo, and J. E. Mooij, *Phys. Rev. Lett.* **95**, 257002 (2005).
- [43] C. Rigetti, A. Blais, and M. Devoret, *Phys. Rev. Lett.* **94**, 240502 (2005).
- [44] Yu-xi Liu, L. F. Wei, J.S. Tsai, and Franco Nori, *Phys. Rev. Lett.* **96**, 067003 (2006).
- [45] Yu-xi Liu, J. Q. You, L. F. Wei, C. P. Sun, and Franco Nori, *Phys. Rev. Lett.* **95**, 087001 (2005).

- [46] P. Bertet, C. J. P. M. Harmans, and J. E. Mooij, Phys. Rev. B **73**, 064512 (2006).
- [47] Y. Makhlin, G. Schon, and A. Shnirman, Nature (London) **386**, 305 (1999).
- [48] J. Siewert, and R. Fazio, Phys. Rev. Lett. **87**, 257905 (2001).
- [49] J. Q. You, J.S. Tsai, and Franco Nori, Phys. Rev. B **68**, 024510 (2003).
- [50] D.V. Averin and C. Bruder, Phys. Rev. Lett. **91**, 057003 (2003).
- [51] D.V. Averin, A.B. Zorin and K.K. Likharev, JETP **61**, 407 (2003).
- [52] J. Lantz, M. Wallquist, V.S. Shumeiko, and G. Wendin, New J. Phys. **7**, 178 (2005).
- [53] B.L.T Plourde, J. Zhang, K. B. Whaley, F. K. Wilhelm, T. L. Robertson, T. Hime, S. Linzen, P. A. Reichardt, C.-E. Wu, and John Clarke, Phys. Rev. B **70**, 140501(R) (2004).
- [54] Alec Maasen van der Brink, A. J. Berkley, and M. Yalowsky, New J. Phys. **7**, 230 (2005).
- [55] M. G. Castellano, F. Chiarello, R. Leoni, D. Simeone, G. Tirolli, and P. Carelli, Appl. Phys. Lett. **86**, 152504 (2005).
- [56] M. G. Castellano, F. Chiarello, R. Leoni, D. Simeone, G. Tirolli, and P. Carelli, cond-mat/0403690 (2004).
- [57] A. O. Niskanen, Y. Nakamura, and J.-S. Tsai, cond-mat/0512238 (2005).
- [58] C. Granata, B. Ruggiero, M. Russo, A. Vettoliere, V. Corato, and P. Silvestrini, Appl. Phys. Lett. **87**, 172507 (2005).
- [59] Mun Dae Kim, Phys. Rev. B **74**, 184501 (2006).

- [60] T. V. Filippov, S. K. Tolpygo, J. Mannik, and J. E. Lukens, IEEE Transactions on Applied Superconductivity, Vol. **13**, No. 2, 1005, (2003).
- [61] A. Romito, R. Fazio, and C. Bruder, Phys. Rev. B **71**, 100501(R) (2005).
- [62] A. Lyakhov and C. Bruder, New J. Phys. **7**, 181 (2005).
- [63] A. O. Lyakhov and C.Bruder, Phys. Rev. B **74**, 235303 (2006).
- [64] D. Burgarth, V. Giovannetti, and S. Bose, quant-ph/0610018, (2006).
- [65] C. H.Bennett and D. P. DiVincenzo, Nature **404**, 247 (2000).
- [66] M. Lewenstein, D. Bruss, J. I. Cirac, B. Kraus, M. Kus, J. Samsonowicz, A. Sanpera, and R. Tarrach, J. Mod. Optics **47**, 2841 (2000).
- [67] M. Beaudry, J. M. Fernandez, and M. Holzer, Theor. Comp. Science **345**, 206 (2005).
- [68] D. Braun and B. Georgeot, Phys. Rev. A **73**, 022314 (2006).
- [69] L. Arnaud and D. Braun, Phys. Rev. A **75**, 062314 (2007).

Curriculum Vitae

Andriy Lyakhov

November 20, 1982

Ukraine

EDUCATION

- Nov 2003 - Nov 2007 BASEL UNIVERSITY, PhD in theoretical physics in the
group of Prof. Dr. Christoph Bruder (magna cum laude)
- Sep 1999 - Oct 2003 CHERNIVTSI NATIONAL UNIVERSITY (Ukraine)
M. S. in Physics (cum laude)
- Sep 1999 - Oct 2003 CHERNIVTSI NATIONAL UNIVERSITY (Ukraine)
M. S. in Computer Systems and Networks (cum laude)
- Sep 1993 - May 1999 SECONDARY SCHOOL (Gymnasium), Chernivtsi (Ukraine).
Graduated with gold medal and honour degree (cum laude)

PUBLICATIONS

- A. Lyakhov, D. Braun and C. Bruder, Phys. Rev. A 76, 022321 (2007)
- Lyakhov and C. Bruder, Phys. Rev. B 74, 235303 (2006)
- A. Lyakhov and C. Bruder, New J. Phys. 7, 181 (2005)
- A. O. Lyakhov, E. G. Mishchenko, Phys. Rev. B 67, R041304 (2003)
- B. N. Gritsuyk, A. A. Lyakhov, S. V. Melnichuk, and V. N. Strebezhev,
Technical Physics, Vol. 46, No. 9, 2001, pp. 1121-1124